

Chapter 2

Chemical Composition of Secondary Organic Aerosol Formed from the Photooxidation of Isoprene*

*This chapter is reproduced by permission from “Chemical Composition of Secondary Organic Aerosol Formed from the Photooxidation of Isoprene” by Jason D. Surratt, Shane M. Murphy, Jesse H. Kroll, Nga L. Ng, Lea Hildebrandt, Armin Sorooshian, Rafal Szmigielski, Reinhilde Vermeylen, Willy Maenhaut, Magda Claeys, Richard C. Flagan, and John H. Seinfeld, *Journal of Physical Chemistry A*, 110 (31), 9665–9690, 2006. Copyright 2006 by the American Chemical Society.

2.1 Abstract

Recent work in our laboratory has shown that the photooxidation of isoprene (2-methyl-1,3-butadiene, C_5H_8) leads to the formation of secondary organic aerosol (SOA). In the current study, the chemical composition of SOA from the photooxidation of isoprene over the full range of NO_x conditions is investigated through a series of controlled laboratory chamber experiments. SOA composition is studied using a wide range of experimental techniques: electrospray ionization – mass spectrometry, matrix-assisted laser desorption ionization – mass spectrometry, high-resolution mass spectrometry, online aerosol mass spectrometry, gas chromatography / mass spectrometry, and an iodometric-spectroscopic method. Oligomerization was observed to be an important SOA formation pathway in all cases; however, the nature of the oligomers depends strongly on the NO_x level, with acidic products formed under high- NO_x conditions only. We present, to our knowledge, the first evidence of particle-phase esterification reactions in SOA, where the further oxidation of the isoprene oxidation product methacrolein under high- NO_x conditions produces polyesters involving 2-methylglyceric acid as a key monomeric unit. These oligomers comprise ~ 22–34% of the high- NO_x SOA mass. Under low- NO_x conditions, organic peroxides contribute significantly to the low- NO_x SOA mass (~ 61% when SOA forms by nucleation and ~ 25–30% in the presence of seed particles). The contribution of organic peroxides in the SOA decreases with time, indicating photochemical aging. Hemiacetal dimers are found to form from C_5 alkene triols and 2-methyltetrols under low- NO_x conditions; these compounds are also found in aerosol collected from the Amazonian rainforest, demonstrating the atmospheric relevance of these low- NO_x chamber experiments.

2.2 Introduction

Secondary organic aerosol (SOA) is formed in the troposphere from the oxidation of volatile organic compounds (VOCs), where the resultant low vapor pressure oxidation products partition between the gas and aerosol phases. Recent laboratory experiments have established that SOA formation can also result from the heterogeneous reactions between particle associated substances and relatively volatile species resulting in the formation of high molecular weight (MW) products via oligomerization (polymerization).¹⁻⁵ Until recently, the formation of SOA from the photooxidation of isoprene, the atmosphere's most abundant non-methane hydrocarbon, was considered insignificant.^{6,7} This was largely due to the known volatility of first-generation gas-phase oxidation products, such as methacrolein (MACR), methyl vinyl ketone (MVK), and formaldehyde, from isoprene oxidation in the presence of NO_x, and a previous chamber study that concluded that isoprene oxidation does not lead to SOA formation.⁸ Recent field observations of certain organic aerosol compounds, diastereoisomeric 2-methyltetrols (2-methylerythritol and 2-methylthreitol) and 2-methylglyceric acid, attributable to isoprene oxidation, and the experimental observation that isoprene under highly acidic conditions can lead to the formation of polymeric, humic-like substances through heterogeneous reactions, re-opened the issue of SOA formation from isoprene.^{7,9-13} Subsequent to their ambient identification, Edney et al.¹⁴ and Böge et al.¹⁵ detected 2-methyltetrols in SOA formed from laboratory chamber studies of isoprene.

Recent work in our laboratory has shown that SOA formation from isoprene oxidation can be significant.^{16,17} Extensive experiments were carried out under both low- and high-NO_x conditions using either nitrous acid (HONO) or hydrogen peroxide (H₂O₂)

as the OH radical source. Photooxidation experiments were also conducted using isoprene first-generation gas-phase oxidation products as the VOC precursor. While no aerosol growth was observed from MVK oxidation, SOA formation was observed from MACR at high-NO_x conditions. High molecular-weight (MW) species were observed to form from isoprene oxidation under both low- and high-NO_x conditions.¹⁷ Moreover, SOA yields were observed to exhibit a dependence on the NO_x level. This dependence appears to be attributed to differences in organic peroxy radical (RO₂) chemistry. At high [NO] (i.e. high-NO_x conditions), RO₂ radicals react mainly with NO to produce small alkoxy radicals (RO) that likely fragment into smaller organics, which are expected to be too volatile to partition appreciably to the aerosol phase, or form organic nitrate species (RONO₂). In the absence of NO_x (i.e. low-NO_x conditions), RO₂ radicals instead react with HO₂ radicals (present in the chamber experiments in large quantities from the OH + H₂O₂ reaction) to form organic hydroperoxides, which have been experimentally shown to be important SOA components from other VOC precursors.^{18,19} Hydroperoxides have been suggested to be involved in polymerization in the aerosol phase via reactions with aldehydes to form peroxyhemiacetals.^{18,19}

Although it is now established that OH-initiated oxidation of isoprene leads to SOA, detailed understanding of the chemical reaction pathways leading to the production of isoprene SOA is lacking. Results from chamber studies have elucidated the importance of the further oxidation of MACR as a primary route for SOA formation from isoprene under high-NO_x conditions. Known RO₂ chemistry at low-NO_x conditions leads to the initial gas-phase oxidation products, likely hydroxyhydroperoxides, of isoprene, which upon further oxidation leads to SOA production. Nonetheless, detailed evaluation

of the mechanism of SOA formation from the oxidation of isoprene has not yet been carried out.

In the present work, a suite of offline analytical techniques is used in conjunction with online aerosol mass spectrometry to investigate the detailed chemical composition of SOA from isoprene oxidation. SOA is produced from the photooxidation of isoprene under varying NO_x conditions and is collected onto filters for offline chemical analyses. Offline mass spectrometry (MS) techniques are used to detect organic species from aerosol filter samples, including oligomeric components of isoprene SOA (as detected in prior studies only by online time of flight aerosol mass spectrometry (TOF-AMS) measurements). Tandem MS and gas chromatography (GC)/MS derivatization techniques are employed to structurally elucidate oligomeric components. Organic peroxides are detected and quantified from low- NO_x isoprene SOA using a conventional iodometric-spectroscopic method. Tracer compounds for isoprene oxidation in the ambient atmosphere, as found in the Amazonian rainforest, are detected here for the first time in the low- NO_x chamber experiments. The low- NO_x conditions are most relevant to understanding SOA formation in highly vegetated, remote regions.⁷ In some cases, such as the southeastern US, where atmospheric transport of pollutants from urban areas can influence SOA formation²⁰, conditions closer to those of the high- NO_x experiments may be applicable.

2.3 Experimental Section

2.3.1 Chamber Experiments

Experiments were carried out in Caltech's dual indoor 28 m³ Teflon smog chambers.^{21,22} Experimental protocols are similar to those described previously,^{16,17} so

will be described only briefly here. Most experiments were carried out with hydrogen peroxide (H_2O_2) as the hydroxyl radical (OH) precursor; in some cases, HONO was used instead to demonstrate that the particular OH source has no effect on the outcome of the experiments. For some experiments, ammonium sulfate seed particles were introduced into the chamber (at volume concentrations of $20\text{--}30\ \mu\text{m}^3/\text{cm}^3$) by atomization of a $0.015\ \text{M}$ ammonium sulfate solution. A known concentration of isoprene (or any other precursor, such as MACR) was then introduced by sending air over a measured volume of the pure compound (Aldrich, 99.8%) into the chamber. For $\text{H}_2\text{O}_2/\text{high-NO}_x$ experiments, NO was also introduced into the chamber from a gas mixture (500 ppm gas cylinder in N_2 , Scott Specialty Gases). In low- NO_x experiments, NO was not added and NO_x concentrations were $< 1\ \text{ppb}$. When the isoprene (monitored by gas chromatography – flame ionization detection (GC-FID)), NO_x , and seed concentrations became constant inside the chamber, irradiation by UV lights (centered at 354 nm) was started, initiating the reaction.

SOA volume growth (mm^3/cm^3) was monitored with a differential mobility analyzer (DMA). For quantification of SOA products collected on filter samples, the DMA volumes were used for each experiment to determine the total SOA mass collected. Filter sampling commenced when the particle growth had terminated, i.e. when the aerosol volume had reached its maximum value. Depending on the total volume concentration of aerosol in the chamber, the filter sampling time was 2 to 4 h, which typically resulted in $3\text{--}7\ \text{m}^3$ of total chamber air sampled.

2.3.2 Filter Extractions

Collected Teflon filters (PALL Life Sciences, 47-mm diameter, 1.0-mm pore size, teflo membrane) were extracted in 5 mL of HPLC-grade methanol by 40 min of sonication. The filters were then removed from the methanol sample extracts and archived at -20°C . Each extract was blown dry under a gentle N_2 stream (without added heat) and then reconstituted with 1 mL of a 50:50 (v/v) solvent mixture of HPLC-grade methanol and 0.1% aqueous acetic acid solution. The reconstituted extracts were then stored at -20°C until analysis was performed. In most cases, filter extracts were chemically analyzed within 1–2 days after filter extraction. Lab control filters were extracted and treated in the same manner as samples. Aliquots of each of these filter extracts were analyzed by the four mass spectrometry techniques to follow.

In order to ensure that H_2O_2 was not condensing onto filter media and introducing artifacts in the chemical analyses, several blank filters were collected under dark conditions from the chamber containing typical experimental well-mixed concentrations of isoprene, NO, and ammonium sulfate seed aerosol, sampled for the same duration ($\sim 2\text{--}4$ h) as a sample filter. No significant chemical artifacts or contaminants were observed in the analytical techniques from these blank filters, consistent with the lack of observed aerosol growth under dark conditions.

2.3.3 Liquid Chromatography / Electrospray Ionization – Mass Spectrometry (LC/ESI-MS)

A Hewlett-Packard 1100 Series HPLC instrument, coupled with a single quadrupole mass analyzer and equipped with an electrospray ionization (ESI) source, was used to identify and quantify relatively polar, acidic SOA components. Data were

collected in both positive (+) and negative (–) ionization modes; the quantitative analysis presented here is limited to the negative ionization mode. An Agilent Eclipse C₁₈ column (3.0 x 250 mm) was used to separate the organic species before detection. The eluents used were 0.1% aqueous acetic acid (A) and methanol (B). In the 40-min gradient elution program used, the concentration of eluent B increased from 5% to 90% in 35 min, and then decreased to 5% in 5 min. The total flow rate of the eluent used in the LC/MS analysis was 0.8 mL min⁻¹. Optimum electrospray conditions were found using a 60 psig nebulizing pressure, 3.5 kV capillary voltage, 13 L min⁻¹ drying gas flowrate, and a 330°C drying gas temperature. During the full scan mode of analysis, the cone voltage was set at 60 V, avoiding fragmentation of most species and allowing their detection as deprotonated molecules ([M – H]⁻). During the upfront collision-induced dissociation (CID) mode of analysis, the cone voltage was set to 110 V, resulting in partial fragmentation of the [M – H]⁻ ions. By comparing these two sets of MS data (upfront CID mode to the full scan mode of analysis) and by examining the fragmentation patterns of the species, some structural information on the analyzed species was obtained. This was particularly useful in confirming results from other MS/MS techniques used and for the identification of oligomeric components.

Using a set of six acidic species (*meso*-erythritol, citramalic acid, 2-hydroxy-3-methylbutyric acid, pimelic acid, pinic acid, and suberic acid monomethyl ester) as surrogate standards, this method was also used to quantify the amount of polar acidic species. Filter extraction efficiency was established by standard additions of these surrogate standards to blank filters. On average, the extraction efficiency for each standard was ~ 60% with an estimated error bar of ~ ±15% over the concentration range

used to generate the LC/MS calibration curves. This average extraction efficiency was included in the calculations to quantify identified isoprene SOA products.

As we will note shortly, to investigate the probable importance of a C₄ hydroxy dialdehyde species formed under high-NO_x conditions, selected sample extracts were derivatized using the Girard Reagent P (1-(carboxymethyl)pyridium chloride hydrazide, MW=187) to increase sensitivity for aldehydic species in the (+)LC/MS mode. The Girard Reagent P (GirP) reacts with aldehydes and ketones to form water-soluble hydrazones with a permanently charged pyridine moiety, and water is eliminated in this reaction.²³ The organic unit that adds to aldehydes and ketones has a mass of 152 Da. A series of aldehyde standards, glyoxal (MW=58), succinic semialdehyde (MW=102), and glutaraldehyde (MW=100), were derivatized using the GirP and analyzed with (+)LC/MS. These small polar aldehyde standards typically go undetected using (+)ESI techniques such as in LC/MS; however, upon derivatization they were detected as the singly charged $[M - H_2O + 152(\text{GirP})]^+$ ions (glyoxal was also detected as doubly charged $[M - 2H_2O + 152(\text{GirP})]^{2+}$ ion), where M is the MW of the aldehyde species. These compounds eluted between 1 to 2 min from the LC column, including a derivatized compound corresponding to the proposed C₄ hydroxy dialdehyde species (MW = 102 and $[M - H_2O + 152(\text{GirP})]^+ = 236$).

2.3.4 ESI – Ion Trap Mass Spectrometry (ESI-ITMS)

Aliquots of the filter extracts were also analyzed by a ThermoElectron LCQ ion trap mass spectrometer equipped with an ESI source, via direct infusion. This instrument does not provide chromatographic separation, precluding quantification. Instead, the instrument was used for the qualitative detection of product species. In addition, specific

ions of interest were isolated from the rest of the sample ion matrix and further fragmented to produce product ion mass spectra, aiding in structural elucidation.

Data were collected in both positive and negative ionization modes. As the same species were detected in both modes ($[M - H]^-$ and $[M + Na]^+$ ions), we only present here the data collected under negative ionization; the data collected under positive ionization serve as confirmation of the negative ionization data.

2.3.5 Matrix Assisted Laser Desorption Ionization -Time of flight Mass

Spectrometer (MALDI-TOFMS)

Another aliquot of the filter extract was analyzed on an Applied Biosystems Voyager-DE Pro MALDI-TOFMS instrument. After 6 μ L of each extract had been dried on the steel target plate, the plate was gently brushed with graphite particles, which served as the matrix. The samples were analyzed in the linear mode, in both positive and negative ionization modes. 400-500 laser shots were summed to obtain a representative mass spectrum of each sample. This method was mainly used to assess the molecular weight (MW) range of the aerosol, to detect oligomeric signatures, and to confirm the MWs of species identified by the ESI techniques.

2.3.6 High Resolution ESI-MS

Extracts were also analyzed by a Waters LCT Premier Electrospray time-of-flight mass spectrometer with W geometry in the Department of Chemistry at the University of California, Irvine, operated in the negative ionization mode. Samples were analyzed by flow injection. The calibration was carried out using sodium formate clusters with co-injection of fmoc-amino acids of appropriate mass spiked into the analytical sample for lock-mass corrections to obtain accurate mass for the oligomeric ions with m/z 266, 323,

365, 368, 467, and 470. These ions were only detected in the high-NO_x experiments and elemental compositions were determined with reasonable accuracy (within +/- 5 ppm), and were consistent with other analytical observations (such as ESI-MS/MS and GC/MS derivatization data).

2.3.7 Aerodyne Time of Flight Aerosol Mass Spectrometer (TOF-AMS)

During most chamber experiments, real-time particle mass spectra were collected continuously by an Aerodyne Time of Flight Aerosol Mass Spectrometer (TOF-AMS), and averaged spectra were saved every 5 min. The design and capabilities of the TOF-AMS instrument are described in detail elsewhere.²⁴ Briefly, chamber air enters the instrument through a 100-mm critical orifice at a flowrate of 1.4 cc/s. Particles with a vacuum aerodynamic diameter between 50 and 800 nm are efficiently focused by an aerodynamic lens, passed through a chopper, and then impacted onto a tungsten vaporizer. The chopper can be operated in three modes: (1) completely blocking the beam to gather background mass spectra; (2) out of the beam's path to collect ensemble average mass spectra over all particles sizes; (3) chopping the beam to create size-resolved mass spectra. The vaporizer is typically run at ~ 550°C to ensure complete volatilization of the SOA and the inorganic seed; during several runs the vaporizer temperature was lowered to ~ 160°C to reduce thermally-induced fragmentation of oligomers. Once vaporized, molecules undergo electron ionization at 70 eV and are orthogonally pulsed every 19 ms into the time of flight mass analyzer.

2.3.8 Gas Chromatography / Mass Spectrometry (GC/MS)

Extracts of selected filters were analyzed for polar organic compounds by GC/MS using a method that was adapted from that reported by Pashynska et al.²⁵ The sample workup consisted of extraction of all or half of the filter with methanol under ultrasonic

agitation and derivatization of carboxyl and hydroxyl functions into trimethylsilyl (TMS) derivatives. The extract was divided into two parts; one part was trimethylsilylated while the other part was stored in a refrigerator at 4°C for eventual further analysis. GC/MS analyses were performed with a system comprising a TRACE GC2000 gas chromatograph, which was coupled to a Polaris Q ion trap mass spectrometer equipped with an external ionization source (ThermoElectron, San Jose, CA, USA). A Heliflex[®] ATTM-5MS fused-silica capillary column (5% phenyl, 95% methylpolysiloxane, 0.25 µm film thickness, 30 m × 0.25 mm i.d.) preceded by a deactivated fused-silica precolumn (2 m × 0.25 mm i.d.) (Alltech, Deerfield, IL, USA) was used to separate the derivatized extracts. Helium was used as carrier gas at a flow rate of 1.2 mL min⁻¹. The temperature program was as follows: isothermal hold at 50°C for 5 min, temperature ramp of 3°C min⁻¹ up to 200°C, isothermal hold at 200°C for 2 min, temperature ramp of 30°C min⁻¹ up to 310°C; and isothermal hold at 310°C for 2 min. The analyses were performed in the full scan mode (mass range: m/z 50 – 800), and were first carried out in the electron ionization (EI) mode and subsequently in the chemical ionization (CI) mode. The ion source was operated at an electron energy of 70 eV and temperatures of 200°C and 140°C in the EI and CI modes, respectively. The temperatures of the GC injector and the GC/MS transfer line were 250°C and 280°C, respectively. For chemical ionization, methane was introduced as reagent gas at a flow rate of 1.8 mL min⁻¹. We present here mainly the data collected in the EI mode; the data collected in the CI mode are used if insufficient MW information is obtained in the EI mode.

Selected extracts were also subjected to a hydrolysis/ethylation and/or a methoximation procedure prior to trimethylsilylation. The purpose of the

hydrolysis/ethylation procedure was to confirm the presence of ester linkages, while that of the methoximation procedure was to evaluate the presence of aldehyde/keto groups, in oligomeric SOA. The hydrolysis/ethylation procedure involved reaction of the extract residues with 40 μL of analytical-grade ethanol and 8 μL of trimethylchlorosilane (Supelco, Bellafonte, PA, USA) for 1 h at 60°C. Details about the methoximation procedure can be found in Wang et al.¹²

2.3.9 Gas Chromatography – Flame Ionization Detection (GC-FID)

Quantitative determination of the 2-methyltetrols (i.e. 2-methylthreitol and 2-methylerythritol), the C₅ alkene triols [i.e. 2-methyl-1,3,4-trihydroxy-1-butene (*cis* and *trans*) and 3-methyl-2,3,4-trihydroxy-1-butene] and 2-methylglyceric acid, in selected filters, was performed by GC-FID with a GC 8000 Top instrument (Carlo Erba, Milan, Italy). The sample workup was the same as that for GC/MS analysis except that filter parts were spiked with a known amount of erythritol (Sigma, St. Louis, MO, USA) as an internal recovery standard; it was assumed that the GC-FID responses of the trimethylsilyl derivatives of the analytes and the internal recovery standard were similar. The GC column and conditions were comparable with those used for GC/MS; the column was a CP-Sil 8 CB capillary column (5% diphenyl, 95% methylpolysiloxane, 0.25 μm film thickness, 30 m \times 0.25 mm i.d.) (Chrompack, Middelburg, The Netherlands) and the temperature program was as follows: isothermal hold at 45°C for 3 min, temperature ramp of 20°C min⁻¹ up to 100°C, isothermal hold at 100°C for 10 min, temperature ramp of 5°C min⁻¹ up to 315°C; and isothermal hold at 315°C for 20 min. Measurement of the 2-methyltetrols in the low-NO_x SOA samples was performed after the unstable products

tentatively characterized as 2-methyltetrol performate derivatives had decayed to 2-methyltetrols, i.e. after leaving the reaction mixture for two days at room temperature.

2.3.10 Total Aerosol Peroxide Analysis

The total amount of peroxides in the low-NO_x isoprene SOA was quantified using an iodometric-spectrophotometric method adapted from that used by Docherty et al.¹⁸ to analyze peroxides formed by α -pinene-ozonolysis. The method employed here differed only in the choice of extraction solvent: we used a 50:50 (v/v) mixture of methanol and ethyl acetate, rather than pure ethyl acetate. Calibration and measurements were performed at 470 nm on a Hewlett-Packard 8452A diode array spectrophotometer. A standard calibration curve was obtained from a series of benzoyl peroxide solutions. Benzoyl peroxide was the standard used for quantification of organic peroxides formed from low-NO_x experiments, as its MW is close to the average MW determined from the mass spectrometry techniques, in particular the MALDI-TOFMS measurements. The molar absorptivity determined from the standard curve was ~ 852 , in excellent agreement with that determined by Docherty et al. and with the value of 845 determined with the original method development paper.^{18,26} As a confirmation that the technique was reproducible, we extracted and analyzed in the same fashion, three α -pinene-ozonolysis filters collected from our laboratory chambers. We measured $\sim 49\%$ of the SOA mass, produced from α -pinene ozonolysis, to be organic peroxides, in excellent agreement to that of Docherty et al.'s measurement of $\sim 47\%$ for the same system. A few high-NO_x isoprene filter samples were also analyzed by this method, but resulted in the detection of no organic peroxides (below detection limits of this technique).

2.3.11 Particle-Into-Liquid Sampler Coupled to Ion Chromatography (PILS/IC)

The PILS/IC (particle-into-liquid sampler coupled to ion chromatography) is a quantitative technique for measuring water-soluble ions in aerosol particles. The PILS developed and used in this study²⁷ is based on the prototype design²⁸ with key modifications, including integration of a liquid sample fraction collector and real-time control of the steam injection tip temperature. Chamber air is sampled through a 1-micrometer cut-size impactor and a set of three denuders (URG and Sunset Laboratories) to remove inorganic and organic gases that may bias aerosol measurements. Sample air mixes with steam in a condensation chamber where rapid adiabatic mixing produces a high water supersaturation. Droplets grow sufficiently large to be collected by inertial impaction before being delivered to vials held on a rotating carousel. The contents of the vials are subsequently analyzed off-line using a dual IC system (ICS-2000 with 25 mL sample loop, Dionex Inc.) for simultaneous anion and cation analysis. The background levels of individual species (Na^+ , NH_4^+ , K^+ , Mg^{2+} , Ca^{2+} , SO_4^{2-} , Cl^- , NO_2^- , NO_3^- , oxalate, acetate, formate, methacrylate, pyruvate) concentrations for analyzed filter samples, presented as the average concentration plus three times the standard deviation (σ), are less than 0.28 mg m^{-3} .

2.4 Results

As noted, experiments were conducted at high- and low- NO_x conditions. High- NO_x conditions were achieved through the addition of substantial NO_x (~ 800 to 900 ppb NO_x) to the reaction chamber, leading to isoprene: NO_x molar ratios of ~ 0.56 to 0.63 . Under low- NO_x conditions no NO_x is added to the chamber, where NO_x mixing ratios of $< 1 \text{ ppb}$ (small amounts of NO_x likely desorb from chamber walls) were observed. The low- NO_x condition simulates a remote (NO_x -free) atmosphere; for example, at typical

isoprene and NO_x mixing ratios observed in the Amazonian rainforest (~ 4 to 10 ppb and 0.02 to 0.08 ppb, respectively),^{7,29} the isoprene:NO_x ratios that result are ~ 50 to 500, comparable to the isoprene:NO_x ratio of the present experiments (~ 500).

2.4.1 High-NO_x Condition

Table 2.1 lists nine high-NO_x chamber experiments that were conducted to generate SOA for aerosol filter sampling. All experiments were conducted with 500 ppb of isoprene or MACR in order to produce sufficient aerosol mass for all offline analytical measurements. In most of the experiments conducted, H₂O₂ served as the OH radical precursor; in this manner, initial oxidation of isoprene is dominated by OH. It is estimated that ~ 3–5 ppm of H₂O₂ was used in each of these experiments based upon isoprene decay during irradiation.¹⁷ All of these experiments were conducted at low relative humidity (RH < 5%) in order to limit the uptake of H₂O₂ into the particle phase. In the high-NO_x experiments using H₂O₂ as an OH source, ~ 800 to 900 ppb of NO was injected into the chamber. With the HONO source, lower initial NO concentrations were achieved, as the source of NO was HONO photolysis and a NO_x side-product from the HONO synthesis. Nucleation (seed-free) and ammonium sulfate seeded experiments were also conducted in order to examine if the presence of seed aerosol has an effect on the chemistry observed. In Experiment 6, acidified ammonium sulfate seed (0.015 M (NH₄)₂SO₄ + 0.015 M H₂SO₄) was used to investigate the possible effect of acid catalysis on oligomerization reactions, which has been previously observed to occur for other VOC precursors, such as α-pinene and 1,3,5-trimethylbenzene.^{1,3-5,30} No discernable increase in SOA mass is observed for this acid-seeded experiment (Experiment 6) when

comparing to its corresponding dry-seeded and nucleation (seed-free) experiments (Experiments 5 and 9).

To illustrate the overall chemical composition typically observed under high- NO_x conditions, shown in Figure 2.1a is a first-order $(-)\text{ESI-IT}$ mass spectrum obtained via direct infusion analysis of an isoprene SOA sample collected from Experiment 1. Prior work in our laboratory has shown that most organics detected in the negative ion mode occur as the deprotonated molecules ($[\text{M} - \text{H}]^-$ ions),^{2,3,20} making $(-)\text{ESI}$ sensitive for the detection of polar acidic species. As can be seen in Figure 2.1a, many such species are detected. Observable 102 Da differences between many of the $[\text{M} - \text{H}]^-$ ions and the detection of high-MW species (up to $\text{MW} \sim 470$) indicate the presence of oligomeric species with more than the 5 carbons of the parent isoprene. Organic nitrate species are detected in this spectrum as even-mass $[\text{M} - \text{H}]^-$ ions (m/z 266, 368, and 470).

Figure 2.1b shows, by comparison, a first-order $(-)\text{ESI-IT}$ spectrum, also obtained via direct infusion analysis, for a MACR high- NO_x sample (Experiment 3). Many of the ions detected correspond exactly to those observed from isoprene oxidation (Figure 2.1a). It should be noted that when the MACR, H_2O_2 , and dry ammonium sulfate seed aerosol are well-mixed in the chamber under dark conditions, no aerosol growth is observed, confirming that photooxidation is required to produce SOA. The SOA components formed in this MACR experiment (as shown in Figure 2.1b) extend out to higher MWs than those of isoprene, which is likely a result of the amount of MACR precursor available in this experiment and also owing to the removal of one oxidation step (the oxidation of isoprene).

SOA products detected in Figures 2.1a and Figure 2.1b are confirmed by additional mass spectrometry techniques. Figure 2.2 shows a mass spectrum collected using the MALDI-TOFMS instrument in the positive ion mode for a high-NO_x, seeded isoprene photooxidation experiment (Experiment 9). SOA components observed here are detected mainly as the sodiated molecules ($[M + Na]^+$ ions), which is consistent with our experiences in analyzing polymeric standards, such as aqueous glyoxal, with a graphite matrix. In Figure 2.2, only species that correspond to ions detected in the (–)ESI-IT spectra are highlighted. For example, for the $[M - H]^-$ ion series detected in (–)ESI-IT spectra at m/z 161, 263, 365, and 467, a corresponding $[M + Na]^+$ ion series is detected at m/z 185, 287, 389, and 491, respectively, using MALDI-TOFMS. It should be noted that the (+)-ESI-IT spectra also detected the same ions ($[M + Na]^+$) as those of the MALDI technique, confirming that the species observed in Figures 2.1 and 2.2 are not a result of ionization artifacts specific to individual techniques.

The LC/MS results obtained in the negative ionization mode are used to quantify the SOA components common to all high-NO_x isoprene SOA (as detected in Figures 2.1 and 2.2). Figures 2.3a and 2.3b show total ion chromatograms (TICs) for an isoprene photooxidation experiment (Experiment 2) and a MACR photooxidation experiment (Experiment 4), respectively, both carried out at high NO_x in the absence of seed aerosol. These TICs show that many of the SOA products formed in each system are the same since the retention times (RTs) are comparable and the m/z values of the molecular ion species ($[M - H]^-$) associated with each chromatographic peak are the same. Shown in Figure 2.3c-e are extracted ion chromatograms (EICs) for three organic nitrate species ($[M - H]^-$ at m/z 266, 368, and 470) common to both isoprene and MACR high-NO_x

photooxidation experiments. For each chamber experiment, EICs were used instead of TICs for the quantification of each $[M - H]^-$ ion detected in order to deconvolute any coeluting species. Figure 2.4a shows a mass spectrum recorded for the largest chromatographic peak (RT = 15.7 min) from the EIC of m/z 368 (Figure 2.3d). The m/z 759 ion that is also detected in this mass spectrum is a cluster ion corresponding to $[2M + Na - 2H]^-$; such cluster ions are commonly observed in (-)LC/ESI-MS conditions. In Figure 2.4b is a resultant upfront CID mass spectrum taken for this same chromatographic peak, showing many product ions from the dissociation of m/z 368. The product ion m/z 305 corresponds to a neutral loss of 63 Da, which is likely nitric acid (HNO_3). Another product ion m/z 291 corresponds to neutral loss of 77 Da, likely from the combined losses of a methyl (CH_3) radical and a nitrate (NO_3) radical (or CH_3ONO_2). The neutral loss of 102 Da results in the product ion m/z 266; these types of product ions are used to aid in the structural elucidation of SOA components, and will be discussed subsequently. Owing to the lack of available authentic oligomeric standards, quantification was carried out by using a series of calibration curves generated from surrogate standards (listed in the Experimental section) covering the wide range of RTs for all detected species. Each surrogate standard contained a carboxylic acid group, the likely site of ionization for detected SOA components, except for the meso-erythritol standard. Due to the initial high percentage of aqueous buffer present in the LC/MS gradient, we were able to detect small polar organics, such as 2-methylglyceric acid. In order to quantify this compound, the polyol meso-erythritol, detected as the $[M - H + \text{acetic acid}]^-$ ion, was used. Unlike meso-erythritol, 2-methyltetrols (and other polyols) were not detected using the (-)LC/MS technique. All surrogate standards were within ~

+/- 1.5 min of the RTs of the detected SOA components. Table 2.2 shows the LC/MS quantification results for high-NO_x SOA. Four types of oligomers are quantified here. For ease of comparison, experiments corresponding to the same VOC and OH precursor type are grouped together under the same column heading.

SOA components observed thus far are not artifacts formed on filters and are observed over varying isoprene concentrations, as confirmed by online particle mass spectrometry. Figure 2.5 shows mass spectra collected from three high-NO_x chamber experiments using the Aerodyne TOF-AMS instrument. In these experiments, the TOF-AMS instrument was operated at ~ 160°C to lessen the degree of thermal fragmentation of the high-MW SOA components. Figure 2.5a shows a TOF-AMS spectrum collected for a 50 ppb isoprene, high-NO_x nucleation experiment (not included in Table 2.1 due to insufficient aerosol mass for offline chemical analysis techniques). Even at these isoprene concentrations, high-MW species are detected in the SOA produced. Differences of 102 Da are noted in this spectrum, again indicating the presence of oligomers. The oligomers present here confirm the species detected by the (-)ESI and (+) MALDI techniques (Figures 2.1 and 2.2, respectively), where the observed TOF-AMS ions result from a loss of a hydroxyl (OH) radical from the molecular ion (i.e. a-cleavage of a hydroxyl radical from a carboxylic acid group). ESI detects these oligomers as the $[M - H]^-$ ion and MALDI as the $[M + Na]^+$ ion, so ions measured in the TOF-AMS instrument are lower by 16 and 40 units, respectively. For example, ions of m/z 145, 187, 247, and 289 measured by the TOF-AMS instrument (Figure 2.5), correspond to m/z 161, 203, 263, and 305, respectively, using (-)ESI (Figure 2.1). Four different series of oligomers are highlighted in this spectrum, where ions of the same

oligomeric series are indicated in a common color. Figure 2.5b corresponds to a MACR high-NO_x, dry seeded experiment, in which a filter sample was collected (Experiment 3), showing the same oligomeric signature to that of the low concentration (50 ppb) isoprene experiment. Figure 2.5c corresponds to an isoprene high-NO_x, HONO experiment (Experiment 8). Again, many ions at the same *m/z* values are detected, as those of Figures 2.5a and 2.5b, suggesting the chemical components of the SOA are the same in these samples. Though probably present, oligomeric compounds formed under conditions similar to those of Figure 2.5c were not detected in the original study of SOA formation from this laboratory,¹⁶ as a less sensitive quadrupole AMS was used; such high-MW species were reported in a subsequent study using the TOF-AMS.¹⁷ These online chemical results confirm that the 102 Da differences observed in the offline analytical techniques (ESI and MALDI) are not a result of sample workup or ionization artifacts. Also, these online chemical results suggest that seeded versus nucleation experiments do not lead to significant differences in the chemistry observed, in agreement with the ESI analyses. The OH precursor (HONO or H₂O₂) also does not have a substantial effect on the chemistry observed (i.e. similar products formed, however, abundances may vary), an observation that is also consistent with the offline mass spectrometry analyses.

PILS/IC measurements were carried out for Experiments 1 (nucleation) and 2 (dry seeded). In both experiments the acetate anion was the most abundant organic anion detected (14.72 mg/m³ in Experiment 1 and 23.47 mg/m³ in Experiment 2) followed by the formate anion (1.18 mg/m³ in Experiment 1 and 2.90 mg/m³ in Experiment 2). It should be noted that these two ions elute off the IC column immediately after sample

injection, and there is a possibility that other early-eluting monocarboxylic acid species co-eluted with these two species leading to an overestimate of their mass. In addition, the extent to which the acetate and formate levels quantified here represent decay products from oligomers detected in the particle phase is uncertain. It is likely that a significant fraction of this mass results from the decomposition of oligomers at the sample collection conditions (high water concentrations and temperatures) in the PILS instrument and possibly by the use of potassium hydroxide (KOH) as the eluent for anion analyses in the IC instrument.

GC/MS with TMS derivatization (restricted to carboxyl and hydroxyl groups) was employed to determine the functional groups present within SOA components formed under high-NO_x conditions. Figure 2.6a shows a GC/MS TIC of a high-NO_x isoprene nucleation experiment (Experiment 5). 2-methylglyceric acid (2-MG), detected previously in ambient and laboratory filter samples,^{10,11,13,14} was found to elute from the GC column at 29.08 min. The corresponding EI mass spectrum for this peak is shown in Figure 2.6b. The chemical structure of trimethylsilylated 2-MG, along with its respective MS fragmentation, is also shown in this mass spectrum. Using GC-FID to quantify the amount of 2-MG present in this same sample, it was found that 3.8 mg/m³ was formed, which accounted for ~ 3.7% of the SOA mass. This was consistent with LC/MS measurements of 2-MG from other high-NO_x isoprene nucleation experiments (such as 2.7% of the SOA mass for Experiment 1). A *di*-ester peak was observed to elute from the GC column at 51.59 min. The corresponding EI mass spectrum for this chromatographic peak is shown in Figure 2.6c along with its proposed chemical structure and MS fragmentation pattern.

2.4.2 Low-NO_x Condition

Table 2.3 lists nine low-NO_x chamber experiments. All experiments were conducted with H₂O₂ as the OH radical precursor with no added NO_x. Ozone formation is attributed mainly to residual NO_x emitted by the chamber walls; these O₃ concentrations observed likely have negligible effect on the gas-phase chemistry due to the slow reactivity of O₃ towards isoprene. Experiments were conducted with 50% of the light banks in the chamber except for Experiments 10 and 11, in which 100% of the light banks were used and resulted in the higher temperatures observed. All experiments were conducted with 500 ppb of isoprene except for Experiment 17, in which 100 ppb of isoprene was used. Nucleation (seed-free) and seeded (ammonium sulfate and acidified ammonium sulfate) experiments were conducted in order to examine if the presence of seed aerosol has an effect on the chemistry observed. Assuming a density $\sim 1.25 \text{ g/cm}^3$ (derived from the comparison of DMA aerosol volume and TOF-AMS aerosol mass measurements), acid seeded (0.015 M (NH₄)₂SO₄ + 0.015 M H₂SO₄) experiments formed the largest amounts of SOA mass ($\sim 259 \text{ mg/m}^3$ for Experiment 14) compared to the corresponding nucleation ($\sim 72.5 \text{ mg/m}^3$ for Experiment 12) and ammonium sulfate seeded experiments ($\sim 72.8 \text{ mg/m}^3$ for Experiment 15). Lower mixing ratios of isoprene (Experiment 17) in the presence of acid seed also resulted in larger amounts of SOA when compared to the nucleation and ammonium sulfate seeded experiments.

No particle-phase organics were detected using (–) and (+)ESI techniques. Analysis of filter sample extracts using these techniques were nearly identical to the blank and control filters. This shows that SOA components at low-NO_x conditions are not acidic in nature like those of the high-NO_x SOA. Due to the expected presence of

hydroperoxides and polyols, other analytical techniques, such as the iodometric-spectrophotometric method and GC/MS with TMS derivatization, were employed to understand the chemical nature of low- NO_x SOA. The peroxide aerosol mass concentration was measured for all experiments except for Experiments 12, 13, and 16. The iodometric-spectrophotometric method measures the total peroxide content (sum of ROOH , ROOR , and H_2O_2) of the aerosol, but because no peroxides were measured from filters collected from air mixtures containing isoprene, H_2O_2 , and seed aerosol, it is assumed that the peroxides measured are organic peroxides. The nucleation experiments (Experiments 10 and 18a) had the highest contribution of peroxides ($\sim 61\%$ on average) to the SOA mass observed. Dry ammonium sulfate (Experiments 11 and 15) and acidified ammonium sulfate seeded experiments (Experiments 14 and 17) led to comparable contributions of organic peroxides to the overall SOA mass (~ 25 and 30% , respectively). Quality control tests were conducted by the addition of ammonium sulfate to standard solutions of benzoyl peroxide to test if the seed had an effect on the UV-Vis measurement of total peroxides. The amount of ammonium sulfate added to the benzoyl peroxide standards was determined by the ratio of SOA volume growth to the typical ammonium sulfate seed volume employed ($\sim 3:1$) as determined from the DMA. Little difference was observed ($\sim 0.6\%$), showing that ammonium sulfate seed has a negligible effect on the measurement of peroxide content from seeded experiments. In most cases, the RHs were $< 9\%$ except during Experiment 15 ($\text{RH} = 25\%$) and Experiment 18b (late sampling, $\text{RH} = 13\%$). Even for these higher RH experiments, no large differences were observed in the fraction of peroxides formed compared to the lower RH experiments. As observed previously¹⁷, the SOA mass was found to decrease rapidly in nucleation

experiments after reaching peak growth, and as a result, the peroxide content of the SOA was measured at different times in Experiment 18. The iodometric-spectrophotometric measurement made at the peak growth in the aerosol volume, as determined from the DMA, for Experiment 18, showed that the peroxides accounted for $\sim 59\%$ of the total SOA mass. Twelve hours later, once the aerosol volume decay reached its constant value, the peroxide contribution to the SOA mass is found to have dropped to 26%.

Figure 2.7 shows a (+)MALDI mass spectrum for a low- NO_x acid-seed experiment (Experiment 14). The m/z range (49 – 620) of ion species observed was not significantly different from (+)MALDI results obtained for nonacid-seeded experiments. The abundances of these ions were higher for the acid experiments, but quantification of these species is not possible due to uncertainties in the ionization efficiencies. In the absence of seed MALDI signal was low or non-existent, likely due to very low ionization efficiencies in the absence of a sulfate matrix. Quantification is also difficult with MALDI because of inconsistencies and inhomogeneities of sample preparation and lack of understanding of sample matrix effects.³¹ It is clear, however, that oligomerization occurs in low- NO_x SOA. Common 14, 16, and 18 Da differences are observed between many peaks throughout this spectrum. Structural elucidation of these peaks in Figure 7 was not possible using the (+)MALDI technique owing to the inability of performing MS/MS experiments on selected ions from the sample matrix.

Figure 2.8 shows two TOF-AMS mass spectra for a 500 ppb, low- NO_x nucleation experiment (Experiment 12) in the m/z range of 200 – 450. These mass spectra also indicate the existence of oligomeric components for low- NO_x SOA. The mass spectrum in Figure 2.8a was collected at a low vaporizer temperature ($\sim 150^\circ\text{C}$) while that in

Figure 2.8b was collected at a higher temperature ($\sim 600^{\circ}\text{C}$). The presence of more higher-mass peaks at high vaporizer temperatures (Figure 2.8b) may indicate that the low- NO_x oligomers are heterogeneous, with some series of oligomers being easily volatilized below 200°C while others are not volatile at these temperatures.

The chemical composition of the SOA formed under low- NO_x conditions was found to change over the course of the experiment. The evolution of selected ions and of the total organic mass measured by the TOF-AMS instrument is shown in Figure 2.9. All ion signal intensities shown here are divided by the signal intensity of sulfate to correct for loss of particle mass to the chamber walls. Figure 2.9a shows the evolution of two prominent high-mass fragment ions m/z 247 and 327. These high-mass fragment ions increase in abundance with time, with the increase in m/z 327 being more significant. This increase is observed for all high-mass ($m/z > 200$) fragment ions. Figure 2.9b shows the change in the intensity of the fragment ion m/z 91, which is proposed to serve as a tracer ion for peroxides formed under low- NO_x conditions, where the proposed formula for this fragment ion is $\text{C}_3\text{H}_7\text{O}_3$, and the structure for one of its isomers is shown in Figure 2.9b. This peroxide tracer ion reaches its maximum signal after seven hours have elapsed in the experiment. Over the next six hours this ion decreases to a lower constant value; such a loss cannot be attributed to wall loss processes since the m/z 91 signal has already been normalized to the sulfate signal. Figure 2.9c shows the time evolution of the organic mass from Experiment 13. The organic mass also slightly decreases after reaching its peak value; however, the decrease observed for the organic mass is much lower than that of the peroxide tracer ion (m/z 91).

PILS/IC data were collected for some low-NO_x experiments. Aerosol mass concentrations of acetate were much lower than in the high-NO_x case. For example, for Experiment 12, acetate anion accounted for only 1.67 mg/m³, ~ 14–22 times lower than that of high-NO_x levels. Formate anion was detected at comparable mass concentrations to that of the high-NO_x experiments (~ 1.51 mg/m³). Again, it should be noted that these two ions elute off the IC column immediately after sample injection and there is a possibility that other early-eluting monocarboxylic acid species co-eluted with these two species, leading to an overestimate of their mass. No other organic anions were detected at significant levels from these low-NO_x experiments.

Figure 2.10a shows a GC/MS TIC of a low-NO_x, dry ammonium sulfate seeded experiment (Experiment 13). The chromatographic peaks at RTs = 31.21, 32.25, and 32.61 min correspond to isomeric C₅ alkene triol species (*cis*-2-methyl-1,3,4-trihydroxy-1-butene, 3-methyl-2,3,4-trihydroxy-1-butene, *trans*-2-methyl-1,3,4-trihydroxy-1-butene, respectively), which have been previously measured in ambient aerosol from the Amazonian rainforest and Finnish boreal forests.^{11,12} This is the first detection of these species in a controlled laboratory chamber experiment. The chromatographic peaks at RTs 38.22 and 38.97 min correspond to the 2-methyltetrols (2-methylthreitol and 2-methylerythritol, respectively), which also have been detected in ambient aerosol studies,^{7,10,11,13} as well as in one previous photooxidation chamber study.¹⁴ The C₅ alkene triols and 2-methyltetrols have received much attention in prior studies; the corresponding mass spectra for their respective chromatographic peaks can be found in Figure 2.20. GC-FID measurements were made to quantify the 2-methyltetrols and C₅ alkene triols for a low-NO_x dry seeded experiment (Experiment 13-peaks in Figure 2.10a)

and a low-NO_x acid seeded experiment (Experiment 14). It was found that the 2-methyltetrols and C₅ alkene triols accounted for 3.91% and 0.60% of the SOA mass, respectively, for the dry seeded experiment (Experiment 13), and decreased to 0.46% and 0.06% of the SOA mass, respectively, for the acid seeded experiment (Experiment 14). The insert shown in Figure 2.10a is the *m/z* 219 EIC for six isomeric dimers (MW = 254) eluting between 58.8 and 59.2 min. The corresponding averaged EI mass spectrum for these chromatographic peaks is shown in Figure 2.10b. The general chemical structure of the trimethylsilylated dimer, along with its respective MS fragmentation, is also shown in this mass spectrum. The fragmentation pattern shown here indicates that the dimer forms by the reaction of a C₅ alkene triol (indicated by the *m/z* 335 fragment ion) with a 2-methyltetrol (indicated by the *m/z* 219 fragment ion) to form the hemiacetal dimer shown. To confirm the MW of the isomeric hemiacetal dimers eluting between 58.8 and 59.2 min, an averaged CI(CH₄) mass spectrum was also collected and is shown in Figure 2.10c. The MW of the trimethylsilylated dimer (derivatized MW = 686) is confirmed by the [M + H – CH₄]⁺ ion at *m/z* 671. The SOA products that elute at 34.91 and 35.47 min were tentatively characterized as diastereoisomeric 2-methyltetrol performate derivatives, which are unstable and upon reaction in the trimethylsilylation reagent mixture are converted into 2-methyltetrols. Their corresponding EI mass spectra can also be found in Figure 2.20. It should be noted that the peaks labeled *1, *2 and *3 in the GC/MS TIC (Figure 2.10a) were also present in the laboratory controls and were identified as palmitic acid, stearic acid and palmitoyl monoglyceride, respectively. Table 2.4 summarizes all low-NO_x SOA components elucidated by GC/MS.

2.5 Discussion

2.5.1 Gas-Phase Chemistry

Gas-phase oxidation of isoprene is dominated by the reaction with OH.^{16,17} Under high-NO_x conditions, O₃ and NO₃ radicals play only a minor role in the initial oxidation of isoprene as they form only once [NO] approaches zero, by which time most of the isoprene is consumed. Under low-NO_x conditions, O₃ and NO₃ radicals also contribute negligibly to isoprene oxidation. Figure 2.11 shows the initial gas-phase reactions that occur under both low- and high-NO_x conditions. In both cases, the initial oxidation of isoprene occurs by reaction with OH, followed by the immediate addition of O₂ to form eight possible isomeric isoprene hydroxyperoxy (RO₂) radicals (for simplicity, only three are shown).

Under high-NO_x conditions, the isoprene hydroxyperoxy radicals react predominantly with NO; however, they may also react with NO₂ to form peroxy nitrates (ROONO₂, not shown in Figure 2.11), but these are likely unimportant to the formation of isoprene SOA due to their thermal instability. RO₂ + NO reactions result in the formation of either hydroxynitrates or hydroxyalkoxy (RO) radicals. Our observations of organic nitrates in high-NO_x SOA as observed in Figure 2.1 ([M – H][–] ions with even *m/z* values) indicate that these hydroxynitrates are likely SOA precursors. Two of the hydroxyalkoxy radicals decompose into MVK and MACR, where their yields are 32–44% and 22–28%, respectively.^{32–35} The remaining hydroxyalkoxy radical forms a 1,4-hydroxycarbonyl, which may isomerize and dehydrate to form 3-methylfuran.³⁶ SOA formation has been observed from the photooxidation of MACR and 3-methylfuran, indicating that these are SOA precursors (indicated by black boxes in Figure 2.11).¹⁷

However, 3-methylfuran is not expected to contribute greatly to the SOA formed by isoprene oxidation because of its low gas-phase product yield ($< 2\text{-}5\%$).³³⁻³⁵ The higher gas-phase product yields observed for MACR suggest it is the most important SOA precursor from isoprene oxidation under high- NO_x conditions; this is consistent with the similarities of the chemical products observed in isoprene and MACR SOA (Figure 2.1 and Table 2.2). Even though MVK typically has the highest gas-phase product yield observed, it is not a contributor to SOA formation under high- NO_x conditions, as negligible amounts of aerosol was produced from the high- NO_x photooxidation of 500 ppb MVK. Other products of isoprene oxidation under high- NO_x conditions (not shown in Figure 2.11) include C_5 hydroxycarbonyls, C_4 hydroxycarbonyls, and C_5 carbonyls; these may contribute to SOA formation but experimental evidence is currently lacking.

Under low- NO_x conditions, the isoprene hydroxyperoxy radicals react predominantly with HO_2 . These reactions result in the formation of hydroxy hydroperoxides, which are highlighted in dotted boxes to indicate that these species are possible SOA precursors. Under similar reaction conditions, Miyoshi et al.³² observed by IR spectroscopy that hydroperoxides are major gas-phase products from isoprene oxidation under NO_x -free conditions. Aerosol formation was also observed; however, the composition of the resultant aerosol was not investigated.

In contrast to Kroll et al.¹⁶, under the present conditions there may be some contribution ($\sim 10\text{--}30\%$) of $\text{RO}_2 + \text{RO}_2$ reactions under low- NO_x conditions owing to the higher $[\text{isoprene}]_0/[\text{H}_2\text{O}_2]$ ratios used in the current study.³² For simplicity, only the $\text{RO}_2 + \text{RO}_2$ reactions that lead to hydroxyalkoxy radicals are shown in Figure 2.11. As in the high- NO_x case, these hydroxyalkoxy radicals will likely form MVK, MACR, and

hydroxycarbonyls. The $\text{RO}_2 + \text{RO}_2$ reactions not shown can lead to the formation of diols and other isomeric hydroxycarbonyls. As will be discussed subsequently, the diols that result from $\text{RO}_2 + \text{RO}_2$ reactions (not shown) may form SOA as well.¹⁵

2.5.2 High- NO_x SOA

2.5.2.1 Importance of MACR Oxidation

MACR oxidation under high- NO_x conditions produces significant amounts of SOA (Experiments 3 and 4). When comparing the SOA products from isoprene and MACR oxidation at high- NO_x conditions, many of the same products are observed (Figure 2.1). Tandem MS data obtained for selected ions common to both isoprene and MACR samples, like the m/z 368 ion shown in Figure 2.4, produced similar product ion spectra, further indicating that these species are indeed the same. This observation is consistent with our previous proton transfer reaction-mass spectrometry (PTR-MS) studies of isoprene oxidation, which demonstrate a strong correlation between the amount of SOA formed and MACR reacted in the gas phase.^{37,38} In these studies, aerosol growth continued well after isoprene was fully consumed, indicating the likely importance of second- (or later-) generation gas-phase products and/or heterogeneous (particle-phase) reactions. It should be noted that when the MACR, H_2O_2 , and dry ammonium sulfate seed aerosol are well mixed in the chamber before irradiation begins, no aerosol growth is observed. This rules out the possibility of reactive uptake of MACR into the particle phase; instead the oxidation of MACR is a necessary step in SOA formation from the photooxidation of isoprene.

2.5.2.2 Oligomers

Oligomerization occurs in SOA formed under high-NO_x conditions, where both offline and online mass spectrometry techniques (Figures 2.1, 2.2, and 2.5) measure species with much higher MWs than that of the parent isoprene, with characteristic 102 Da differences. Tandem MS techniques, such as upfront CID on the LC/MS instrument, confirm that oligomers are indeed formed from a common 102 Da monomeric unit. For example, when isolating the *m/z* 368 ion from the rest of the sample matrix and further fragmenting it to generate a product ion spectrum, two successive neutral losses of 102 Da were observed at *m/z* 266 and 164 (Figure 2.4b). Two isomeric compounds with *m/z* 266 in Figure 2.3c were found to elute off the LC column at ~ 2.5–3 min earlier than the compound with *m/z* 368 studied here. The fact that the compounds with *m/z* 266 ions elute off the LC column at earlier RTs, and that *m/z* 266 is a product ion of *m/z* 368, strongly suggests that these two ions are characteristic of the same oligomeric series. The compounds characterized by *m/z* 368 and 266 are likely a trimer and dimer, respectively. The other series of oligomers quantified in Table 2.2 also had 102 Da differences observed and similar LC/MS behaviors, with ions with lower mass eluting from the LC column at earlier RTs.

2.5.2.3 Organic Nitrates

Organic nitrates, detected as even-mass $[M - H]^-$ ions in (–)ESI spectra, were measured in all high-NO_x experiments. All organic nitrates detected in high-NO_x SOA samples had similar product ion spectra as *m/z* 368 (Figure 2.4b), with neutral losses of 63 (HNO₃), 77 (CH₃ radical + NO₃ radical, possibly CH₃NO₃), and 102 Da, suggesting that all even-mass $[M - H]^-$ ions are oligomeric organic nitrate species. Unlike the (–)ESI techniques (Figure 2.1 and 2.3), the GC/MS technique did not allow for the

detection of organic nitrate species, likely a result of their instability at the high temperature of the GC injector and/or derivatization techniques used during sample workup. Organic nitrates also were not clearly detected in the MALDI-TOFMS (Figure 2.2) and the TOF-AMS (Figure 2.5) instruments. This is likely a result of the harsh ionization techniques employed by these instruments. Even with (–)ESI, these organic nitrates were not completely stable, as shown in Figure 2.4a for the m/z 368 ion. Organic nitrates found in the high-NO_x SOA likely form from the further oxidation of the hydroxynitrate species found in the gas phase from RO₂ + NO reactions.

2.5.2.4 2-MG as Monomeric Units

As shown in Table 2.2, other varieties of oligomers were observed as well. From further use of tandem MS techniques, it was found that one of these series of oligomers likely involved 2-MG (2-methylglyceric acid), a recently discovered SOA tracer compound for isoprene oxidation in the ambient atmosphere,^{10,13,14} as an important monomer. Confirmation of the 2-MG monomer in high-NO_x SOA was provided by GC/MS with TMS derivatization (Figures 2.6a and 2.6b). Because monomeric 2-MG is small and polar, it was not effectively retained by the LC reverse phase column (RT ~ 1.3 min) and was detected in its deprotonated form at m/z 119. Figure 2.12 shows product ion spectra obtained with (–)ESI-ITMS for Experiment 9. In Figure 2.12a, the m/z 323 ion is isolated in the ion trap from the rest of the ion matrix and is collisionally activated to produce the MS² spectrum shown here. The m/z 221 ion is the base peak in this spectrum, and the m/z 119 ion also detected as the result of further fragmentation of the m/z 221 product ion. The fact that the m/z 119 ion was detected as a product ion in the MS² and MS³ spectra shown in Figure 2.12, strongly suggests that 2-MG is a monomer in

this oligomeric series. It is important to note that m/z 119 was also a fragment ion produced in the upfront CID spectrum for the m/z 368 ion in Figure 2.4b. It was found that m/z 119 was a common product ion to each oligomeric series, suggesting the importance of 2-MG in oligomerization reactions.

2.5.2.5 Mono-Acetate and Mono-Formate Oligomers

The PILS/IC measurements of high levels of particulate acetate and formate anions in both the seeded (Experiment 1) and nucleation (Experiment 2) experiments, coupled with the high volatilities of their acid forms produced in the gas phase from the oxidation of isoprene, suggests that these compounds resulted from the decomposition of oligomeric SOA. The formation of *mono*-acetate and *mono*-formate oligomers was observed by tandem (–)ESI-MS measurements. Figure 2.13 shows two product ion spectra for a *mono*-acetate dimer ($[M - H]^-$ at m/z 161) and *mono*-formate trimer ($[M - H]^-$ at m/z 249), respectively. The observation of a neutral loss of 42 Da (ketene, $H_2C=C=O$) and a dominant product ion m/z 59 (acetate anion) in the MS^2 spectrum of the m/z 161 ion (Figure 2.13a), provides strong evidence for acetylation. In the MS^2 spectrum of the m/z 249 ion (Figure 2.13b), the major product ion m/z 147 results from the common neutral loss of 102 Da. The product ion m/z 221 results from a neutral loss of 28 Da (CO), a rearrangement reaction which is characteristic of formates. The product ion m/z 119 (deprotonated 2-MG) resulting from the combined neutral losses of 102 and 28 Da is also observed. *Mono*-acetate oligomers were also detected by the GC/MS TMS derivatization method; the details of these findings will be discussed in a forthcoming GC/MS complementary paper.

2.5.2.6 Heterogeneous Esterification Reactions

Oligomer species containing the m/z 119, 221, and 323 ions as detected by the (–)ESI techniques were also observed by GC/MS as their respective TMS derivatives as shown Figure 2.6a. As in previous measurements of 2-MG,¹⁴ the EI mass spectrum shown in Figure 2.6b confirms the formation of monomeric 2-MG in high-NO_x isoprene SOA. The dimer detected at m/z 221 by (–)ESI techniques (as shown in Figure 2.12b) involving 2-MG as an important monomer, is detected at 51.59 min in Figure 2.6a. The chemical structure of this species likely contains 1 carboxyl and 3 hydroxyl groups, as shown in Figure 2.6c. The formation of an ester linkage is also denoted in this structure, which is the expected site of oligomerization. The ions m/z 583 ($[M + \text{TMS}]^+$) and m/z 495 ($[M - \text{CH}_3]^+$) confirm that the MW of this dimer species is 222 (which is also in agreement with the ESI results). The ion m/z 467 ($[M - (\text{CH}_3 + \text{CO})]^+$) is consistent with a terminal trimethylsilylated carboxylic group, while the ion m/z 480 ($[M - \text{CH}_2\text{O}]^+$) is explained by a rearrangement of a trimethylsilyl group and points to a terminal trimethylsilylated hydroxymethyl group. The elemental composition (C₈H₁₄O₇) of the structure shown in Figure 2.6c was also confirmed by high-resolution ESI-TOFMS measurements. These results strongly suggest that particle-phase esterification reactions occurred between 2-MG molecules, where a hydroxyl group of one 2-MG molecule reacted with a carboxylic acid group of another one. The products that result from this reaction would be the ester compound shown in Figure 2.6c and a water molecule. The neutral loss of 102 Da, likely corresponding to dehydrated 2-MG or a 2-MG residue in the form of a lactone (i.e. 2-hydroxy-2-methylpropiolactone), observed from the ESI-MS/MS techniques can be explained by the charge-directed nucleophilic reaction shown

in Figure 2.14. To our knowledge, this is the first evidence of particle-phase esterification reactions in SOA. It should be noted that the mass spectra, not shown here, for the chromatographic peaks in Figure 2.6a at 60.01 and 60.31 min, correspond to branched and linear 2-MG acid trimers (corresponding to MW = 324), respectively. A detailed discussion of the EI mass spectral behavior of the TMS derivatives of 2-MG, 2-MG dimer and trimers will be presented in a complimentary GC/MS study.

Figure 2.15a and 2.15b compares the GC/MS EICs, using the m/z 219 ion as the base peak, for a filter sample from Experiment 5 treated with trimethylsilylation only to that of a filter sample (also from Experiment 5) treated by hydrolysis/ethylation + trimethylsilylation, respectively, to show further confirmation of polyesters formed via esterification reactions between 2-MG molecules. When treating SOA from the same chamber experiment with the hydrolysis/ethylation procedure, a noticeable decrease in 2-MG and 2-MG oligomers is observed. For example, the peaks at 29.08, 51.59, and 60.31 min (Figure 2.15a) observed after trimethylsilylation appear as smaller peaks upon the hydrolysis/ethylation experiment, as shown in the second chromatogram (Figure 2.15b). This decrease is a result of the formation of ethyl esters of 2-MG and of linear dimer (RTs = 27.42 and 50.48 min, respectively). The mass spectra confirming the formation of these ethyl ester species are shown in Figures 2.15c and 2.15d, respectively. The m/z 365 and 277 ions in Figure 2.15c confirm the MW of the ethyl ester of 2-MG to be 148, where its formation is the resultant of polyesters decomposing into this derivatized monomer. The detection of m/z 539 and 451 in Figure 2.15d confirm the MW of the ethyl ester of the linear 2-MG dimer, likely a result of the incomplete decomposition of larger polyesters (i.e. trimers, tetramers, pentamers, etc.) in high- NO_x SOA.

Figure 2.16 shows the overall proposed reaction mechanism for SOA formation from the photooxidation of isoprene under high- NO_x conditions. This figure denotes important initial gas- phase and particle-phase reactions that lead to the observed SOA products. As was discussed earlier, further gas-phase oxidation of MACR is required in order to form SOA from isoprene under high- NO_x conditions. Oligomeric organic nitrates, such as the m/z 368 ion, are comprised of an organic nitrate monomer, which is detected as the deprotonated m/z 164 product ion (Figure 2.4b); therefore, it is possible that one gas-phase product of MACR oxidation is its hydroxynitrate form, as shown in Figure 2.16. Through further oxidation of the aldehyde group in this hydroxynitrate species, it is expected that the acid form of this species results in the particle phase, thus being available for esterification reactions with 2-MG (Reaction 2 in Figure 2.16). To our knowledge, no organic nitrates have been measured in the gas phase from MACR oxidation (though nitrate formation has been inferred from OH-methacrolein reaction kinetics³⁹); however, the detection of organic nitrates in the particle phase suggests that this is possibly a minor channel for SOA formation. On the other hand, the formation of 2-MG from the oxidation of MACR is still uncertain, due to the unknown intermediates leading to its formation. Recently, it was proposed that 2-MG forms from the reaction of methacrylic acid or MACR with H_2O_2 in the liquid aerosol phase under acidic conditions.¹³ No aerosol growth was observed for MACR, H_2O_2 , and dry ammonium sulfate seed aerosol under dark conditions, however, it is possible that other products such as formic and acetic acid, as well as oxidants formed during isoprene photooxidation, may promote the reactive uptake of MACR into the aerosol phase.

Further measurements of MACR oxidation products are needed in order to better understand the formation of 2-MG, which might occur in either the particle or gas phase.

From our detailed analytical measurements discussed above, the importance of 2-MG to particle-phase reactions in high-NO_x SOA is now well established. 2-MG monomers can react intermolecularly via esterification to produce 2-MG oligomers (Reaction 1), or react with *mono*-nitrate monomers to produce *mono*-nitrate oligomers (Reaction 2), or react with acetic or formic acid to produce *mono*-acetate and *mono*-formate oligomers, respectively (Reactions 3 and 4). These proposed esterification reactions are equilibrium reactions, and as a result, the addition of an acid or removal of water could promote the formation of these esters. As stated earlier, the high-NO_x experiments were conducted at very low relative humidities (RH < 5%); therefore, this condition could allow for the ester formation we observe. We also observe high concentrations of organic acids (2-methylglyceric, acetic, and formic acid) at the high-NO_x condition, which could provide the acidity needed to drive these reactions. It has been shown⁴⁰ that heterogeneous esterification of polyols by vapor-phase treatment with acetic acid and trifluoroacetic anhydride (used as an alternative to the sulfuric acid catalyst) will occur at room temperature without the use of liquids. Thus it is reasonable to infer that esterification reactions may occur under the dry, room temperature conditions of our chamber experiments. It should be noted that there is also evidence from the TOF-AMS that supports this reaction mechanism. The ratio of the TOF-AMS ion signals associated with the 2-MG dimer (m/z 205) to that of the 2-MG monomer (m/z 103) increases during the course of the high-NO_x experiments; therefore, providing additional confirmation of our proposed reaction mechanism in Figure 2.16. These

results from the TOF-AMS, however, are not quantitative due to the majority of these molecules being fragmented (thermally or by the electron impact ionization) to smaller ions.

In comparison to MACR oxidation, the further oxidation of MVK likely does not produce SOA under high-NO_x conditions due to its ketone moiety. The lack of an aldehydic hydrogen precludes the formation of acidic products (like that of 2-MG from MACR oxidation), which are necessary components needed for the particle-phase esterification reactions (Figure 2.16). One of the most abundant gas-phase products produced from MVK oxidation under the high-NO_x condition is methylglyoxal. It was shown in a prior chamber study by Kroll et al.⁴¹ that methylglyoxal does not reactively uptake onto inorganic seed aerosol; therefore, this could explain the lack of SOA growth from the further oxidation of MVK.

For the isoprene/H₂O₂ experiments, except for Experiment 6, the most abundant oligomer series was the *mono*-nitrate oligomers (Table 2.2). The *mono*-nitrate oligomers accounted for ~ 8–13% of the SOA mass formed in these experiments. As for the isoprene/H₂O₂ experiments, the *mono*-nitrate oligomers were the most abundant oligomers for the MACR/H₂O₂ experiments (~ 35% of SOA mass for seeded experiment vs ~ 20% for nucleation experiment). Even though most of the chemical products are the same in the H₂O₂ and HONO experiments, the abundances of these products are different. In contrast to the H₂O₂ experiments, the 2-MG oligomers are the most abundant oligomers for the HONO experiments. These differences could be due to different NO_x levels. SOA mass closure was observed to be the highest for the MACR/H₂O₂/seeded experiment (~57% of SOA identified) and the isoprene/H₂O₂/seeded

experiments (22–34% identified). It is important to stress that the organic aerosol mass loadings formed in these isoprene high-NO_x chamber experiments ($\sim 50 - 200 \mu\text{g m}^{-3}$) are much higher than those found in ambient aerosol where isoprene emissions are the highest ($\sim 5 \mu\text{g m}^{-3}$). The amount of organic aerosol mass controls the gas-particle partitioning of semi-volatile species produced from the oxidation of hydrocarbons, as more organic aerosol mass allows for more uptake of these species; therefore, the mass closure results presented apply only to the aerosol mass loadings produced in this current study and are not absolute for the isoprene system. The key insight from our analysis is the detection of these various oligomeric products formed from particle-phase esterification reactions.

2.5.2.7 Additional Routes for SOA Formation

As shown in Table 2.2, the polyester products from oligomerization of 2-MG and related components account only for a portion (22–34%) of the SOA formed from isoprene oxidation under high-NO_x conditions. This lack of mass closure could result from the LC/MS technique underestimating the amount of polyesters, possibly related to the use of a C₁₈ reverse phase column and the unavailability of authentic standards. The C₁₈ reverse phase column could have degraded the oligomers into smaller units as they pass through the column, or very large oligomers could have permanently been retained onto the reverse phase material, and hence were not detected. Negative bias associated with filter sampling, such as evaporative losses during sampling or storage, could also be a source of incomplete mass closure. The presence of acetic acid in eluent mixture used for the LC/MS runs could also have caused an underestimation of the oligomers formed due to the possibility of acid-catalyzed hydrolysis during ESI, a process that would lead

to a decrease in the detection of oligomeric compounds. Besides possible errors associated with quantifying esterification products identified by the LC/MS technique, the possibility still exists that other unidentified second- (or later-) generation gas- or particle-phase products from isoprene oxidation contribute to SOA formation, and as a result, would increase the mass closure significantly.

Glyoxal, a C₂ dialdehyde, has been recently shown to be reactively taken up into particulate matter,^{41,42} however, not at the low RHs employed in this study (RH < 5%). Theoretically, it has been shown that this reactive uptake of glyoxal results from thermodynamically favorable hydration and oligomerization.^{43,44} When first interpreting the MS data from the ESI and MALDI techniques, it was considered that a dialdehyde species possibly corresponded to the 102 Da neutral losses observed from the oligomeric components. Figure 2.17 shows a proposed gas-phase reaction scheme for the formation of a C₄ hydroxy dialdehyde species (MW=102) from the further oxidation of MACR. In contrast to glyoxal, dissolution may not be required for this proposed dialdehyde species to form SOA; therefore other heterogeneous processes may occur. The detailed analysis of the GC/MS derivatization and the ESI tandem MS results, however, provides strong chemical evidence for the formation of polyesters, where the neutral loss of 102 Da is explained by the dehydrated lactone form of 2-MG (Figure 2.14). In addition, a GC/MS derivatization analysis made for MACR high-NO_x SOA (Experiment 3) that included a methoximation step prior to trimethylsilylation to reveal aldehyde functions in the formed oligomers was negative.

To investigate further the probable importance of a C₄ hydroxy dialdehyde species and its respective hemiacetal oligomers, selected sample extracts were derivatized using

the Girard Reagent P to increase sensitivity for aldehydic species in the (+)ESI mode. A high-NO_x isoprene and MACR sample were treated with this derivatizing agent, and as a result, the detection of the *m/z* 236, 206, and 192 ions resulted for both samples, which likely corresponds to the detection of the proposed C₄ dialdehyde, glyoxal, and methylglyoxal, respectively. However, the proposed hemiacetal oligomers that would be produced from this C₄ dialdehyde were not detected, consistent with observations made in the methoximation GC/MS experiment. It is possible that the detection of the proposed C₄ dialdehyde resulted from the decomposition of oligomers during the derivatization step of the sample workup procedure (which is equivalent for the detection of glyoxal and methylglyoxal in the particle phase). As a confirmation that the observed ions were derivatized species of the proposed C₄ dialdehyde, glyoxal, and methylglyoxal, upfront CID LC/MS analysis was used to detect common neutral mass losses and fragment ions associated with derivatized aldehydes and ketones. The common neutral losses and fragment ions associated with the GirP derivatization detected were similar to those found by Lai et al.,²³ providing further evidence of the detection of these small aldehyde species in high-NO_x isoprene and MACR SOA. The detection of these small dicarbonyls provides some evidence that aldehydes may account for a fraction of the unquantified (unidentified) SOA mass (Table 2.2) produced from isoprene oxidation under high-NO_x conditions. The mechanism (reactive uptake and/or oligomerization) and the degree in which these aldehydes form SOA, however, remains unclear and bears further study.

2.5.3 Low-NO_x SOA

2.5.3.1 Hydroperoxides: Key Component to SOA Formation

As discussed previously, in the absence of NO_x , the RO_2 radical chemistry is dominated by $\text{RO}_2 + \text{HO}_2$ reactions, owing to the large amounts of HO_2 formed from the $\text{OH} + \text{H}_2\text{O}_2$ reactions.¹⁷ $\text{RO}_2 + \text{RO}_2$ reactions are expected to be less substantial (10–30% contribution) due to the high HO_2/RO_2 ratios in these experiments, and as a result, hydroperoxides are expected to be the dominant gas-phase products. Due to their expected low volatilities, hydroperoxide species can partition to the aerosol phase and likely form high-MW species via peroxyhemiacetal formation with aldehydic species.^{18,19} Hydroperoxides resulting from the oxidation of aromatic and biogenic VOCs have been observed and calculated to be important contributors to the overall SOA mass.^{18,45,46} Indeed, as shown in Table 2.3, organic peroxides (i.e. hydroperoxides or ROOR) also are a significant component (~ 61% of the SOA mass for nucleation experiments and ~ 25% and 30% of the SOA mass for dry seeded and acid seeded experiments, respectively) of the low- NO_x isoprene SOA. The large discrepancy in peroxide content observed between nucleation (seed-free) and seeded experiments is currently not understood. As discussed in the results section, there is no evidence of interference from ammonium sulfate on the peroxide content measurement. Owing to the neutral nature of the hydroperoxides (and ROOR) measured by the iodometric-spectrophotometric method, no tandem ESI-MS measurements could be made to structurally elucidate this fraction. Thus, it is difficult to explain the differences in the peroxide content observed between nucleation and seeded experiments. It is possible that in the seeded cases the hydroperoxide species are heterogeneously converted into neutral species other than peroxidic compounds, such as polyols. Further studies should be conducted to investigate the role of inorganic seed on the amount of peroxides formed in the aerosol phase. As noted in the high- NO_x case, the

mass closure results presented here apply only to the aerosol mass loadings produced in this current study and can not be concluded as absolute for the isoprene system at low- NO_x conditions.

2.5.3.2 Oligomerization

Oligomers were found to form under low- NO_x conditions, as shown in the (+)MALDI (Figure 2.7), GC/MS with TMS derivatization (Figure 2.10), and TOF-AMS (Figures 2.8 and 2.9) data. In contrast to high- NO_x conditions, no distinct pattern or obvious monomeric unit, like the 102 Da differences observed in the high- NO_x oligomeric SOA (Figures 2.1, 2.2, and 2.5), was observed in the low- NO_x oligomers. The oligomers formed in the low- NO_x case are not acidic in nature like in the high- NO_x case. Structural elucidation of these oligomers is limited, as these neutral products are not ionizable using ESI-MS. MALDI (Figure 2.7) was able to provide some indication of the MW ranges of the oligomeric SOA, but structural elucidation was not possible. The large mass contribution of organic peroxides to the low- NO_x SOA (Table 2.3) provides some insight into the oligomerization reactions occurring. It is possible that some fraction of the oligomeric SOA is formed by peroxyhemiacetals, which result from heterogeneous reactions of hydroperoxides and aldehydes.

Due to the neutral nature of the oligomeric SOA produced under low- NO_x conditions, only the GC/MS derivatization technique provides structural elucidation of the oligomers formed owing to the presence of polyols. Hemiacetal formation reactions between C_5 alkene triols (Table 2.4) and 2-methyltetrols (Table 2.4) were found to occur using this technique (Figure 2.10b). The reaction involves a terminal hydroxyl group of a 2-methyltetrol, which serves as a nucleophile, reacting with the tautomeric keto form of

one C₅ alkene triol (Table 2.4) to form the hemiacetal dimer shown in Figure 2.10b. As was observed by the GC/MS *m/z* 219 EIC, six isomeric forms of this hemiacetal dimer could be partially resolved. However, further elucidation of higher-order hemiacetal (acetal) oligomers could not be conducted owing to their likely thermal decomposition in the GC injector of the GC/MS instrument, their high MW preventing their elution from the GC column, and lack of ionization when using ESI-MS techniques. As for the confirmation of peroxyhemiacetal oligomers, analytical techniques need to be developed in order to further elucidate the neutral higher-order hemiacetal (acetal) oligomers likely present in low-NO_x SOA.

2.5.3.3 Acid Catalysis

The SOA mass for the acid seed experiment (Experiment 17) is significantly larger (~ 3.6 times) than that of the dry seeded/nucleation experiments (Experiments 15/12), in contrast to high-NO_x conditions, in which acid seed had no such observable effect. Note that the SOA mass concentration was virtually identical in experiments using dry (nonacid) seed aerosol and in those in the absence of seed aerosol, where particle formation takes place by nucleation (Experiments 12, 13, and 15). GC-FID measurements made for selected low-NO_x experiments also provide evidence for acid-catalyzed particle-phase reactions. The C₅ alkene triols and 2-methyltetrols decreased in their contributions to the overall SOA mass when acid seed was present. For example, the 2-methyltetrols and C₅ alkene triols contributed ~ 3.91% and 0.6%, respectively, to the SOA mass for Experiment 13 (non-acid case), where as in Experiment 14 (acid case), the 2-methyltetrols and C₅ alkene triols were found to decrease to ~ 0.46% and 0.06%, respectively, of the SOA mass. This result is in contrast to that observed by Edney et

al.¹⁴ in which isoprene tracer compounds were observed to increase in concentration, and is possibly due to the differing isoprene:NO_x ratios employed. In conjunction with the above GC-FID results, the fact that C₅ alkene triols and 2-methyltetrols were found to form hemiacetal dimers (and likely higher order oligomers) suggests that the presence of acidified aerosol catalyzes hemiacetal (and likely acetal) oligomer formation under low-NO_x conditions. The same may be the case for peroxyhemiacetal formation reactions.

2.5.3.4 Formation Mechanism of Low-NO_x SOA products Observed by GC/MS

The detection of organic peroxides in the particle phase (Table 2.3) by the iodometric-spectrophotometric method, provides strong evidence that the hydroperoxides that result from the gas phase RO₂ + HO₂ reactions are sufficiently polar (nonvolatile) to partition to the aerosol phase, thereby elucidating one major reaction pathway leading to SOA formation under low-NO_x conditions. The detection of 2-methyltetrols, C₅ alkene triols, 2-methyltetrol performate derivatives, and hemiacetal dimers (Table 2.4) suggests that the RO₂ radicals that form from the initial oxidation (OH/O₂) of isoprene follow some other route. The formation of 2-methyltetrols has been explained by self- and cross-reactions of the RO₂ radicals formed from the initial oxidation (OH/O₂) of isoprene, leading to intermediate 1,2-diols, which may undergo a second cycle of oxidation (OH/O₂) reactions followed by self- and cross-reactions of the RO₂ radicals.⁷

The detection of C₅ alkene triols in ambient aerosol may indicate the importance of intermediate epoxydiol derivatives of isoprene, which may also be intermediates in the formation of 2-methyltetrols.^{11,12} Wang et al.¹² hypothesized from MS evidence that these epoxydiol intermediates could be trapped in the aerosol phase and subsequently converted into C₅ alkene triols and 2-methyltetrols through acid-catalyzed reactions.

Acid-catalyzed reactions of epoxydiols may be a formation pathway for 2-methyltetrols and C₅ alkene triols, but these monomers may also form from other pathways.

Shown in Figure 2.18 is a proposed mechanism for the formation of key SOA components from the oxidation of isoprene under low-NO_x conditions. As suggested by Böge et al.¹⁵, 2-methyltetrols may form by several possible pathways. The formation of the 2-methyltetrols through two cycles of oxidation (OH/O₂) reactions followed by self- and cross-reactions of the RO₂ radicals is only briefly included in this figure. It is possible that epoxydiols may form from rearrangements of hydroxyhydroperoxides or hydroxyperoxy radicals. Once formed, these epoxydiols could be taken up into the particulate phase, and through hydrolysis form 2-methyltetrols. In addition, an alternative pathway leading to the formation of 2-methyltetrols has been reported in a recent study by Böge et al.¹⁵ That study proposed that intermediates in the formation of 2-methyltetrols (i.e. 2-methyl-3-butene-1,2-diol and 2-methyl-2-vinyloxirane) are converted to 2-methyltetrols through reaction with hydrogen peroxide on acidic particles. The latter pathway is also included in the scheme in Figure 2.18. Further gas and particle-phase studies are needed in order to fully elucidate the pathways leading to the formation of 2-methyltetrols, the C₅ alkene triols and related dimeric products.

2.5.3.5 Evolution of SOA Composition

As in Kroll et al.¹⁷, a rapid decay of the SOA mass was observed after the initial SOA growth reached its maximum for all low-NO_x nucleation experiments. This loss is not attributable to wall removal processes since the particles shrink in size rather than reduce in number (as measured by the DMA). The loss of SOA mass was observed to

stop immediately after chamber lights were turned off, and to resume once the lights were turned back on, indicating a photochemical effect.

Indeed, when comparing the peroxide measurements made at (or around) the initial SOA growth maximum to some later experimental time after SOA mass decay, it was found that the organic peroxide content of the aerosol significantly decreased (~ 59% to 26% of SOA mass, respectively for Experiment 18). This observation provides strong evidence that organic peroxides decompose in the particle phase due to photolysis and/or subsequent particle-phase reactions, or they are driven out of the particle as a result of gas-phase compounds being reacted away, shifting the equilibrium back to the gas phase. TOF-AMS measurements also confirmed that the peroxide content of low-NO_x SOA decreases with time as shown in Figure 2.9b. This decrease in peroxide content as a function of time also coincided with high-mass fragment ions ($m/z > 200$) increasing in their abundance (in Figure 2.9a only m/z 247 and 327 are shown), suggesting the possibility that peroxide decomposition causes oligomerization reactions. These oligomerization reactions likely lead to hemiacetals (as elucidated by GC/MS).

2.5.3.6 Tracer Compounds for Isoprene Oxidation in the Remote Atmosphere

The low-NO_x chamber experiments conducted in this study confirm that 2-methyltetrols indeed serve as tracer compounds for isoprene oxidation in the ambient atmosphere, especially in remote regions such as the Amazonian rainforest. The detection of C₅ alkene triols and hemiacetal dimers in the present low-NO_x experiments corresponds well to their observation in ambient aerosol collected from the Amazonian rainforest¹² and Finnish boreal forests (note that hemiacetal dimers in aerosol collected from the Finnish boreal forests is not yet confirmed).¹¹ From these field studies, C₅ alkene

triols were postulated to form by acid-catalyzed ring opening reactions of epoxydiol derivatives of isoprene in low RH environments. However, hemiacetal dimers were not recognized in ambient samples; this current study elucidates their formation under low- NO_x conditions. Once it was realized that hemiacetal dimers form from C_5 alkene triols and 2-methyltetrols, we referred back to data collected from the Amazonian rainforest.⁴⁷ When investigating the GC/MS data carefully, it was found that the hemiacetal dimers were indeed detected, suggesting the atmospheric relevance of these low- NO_x chamber experiments. Shown in Figure 2.19 is a GC/MS EIC of an Amazonian fine aerosol sample (i.e. $\text{PM}_{2.5}$; particulate matter with an aerodynamic diameter $< 2.5 \mu\text{m}$) collected during the wet season (low- NO_x conditions) using multiple ions, i.e. m/z 231 (to show the C_5 alkene triols), m/z 219 (to show 2-methyltetrols as well as the dimers) and m/z 335 (characteristic of the dimers). An averaged EI mass spectrum for the hemiacetal dimers is also included in this figure to further confirm their presence in ambient aerosol.

2.6 Conclusions

The composition of SOA from the photooxidation of isoprene under both high- and low- NO_x conditions has been thoroughly investigated through a series of controlled laboratory chamber experiments. It is found that the chemical nature of the resultant SOA is significantly different in the two NO_x regimes. Under high- NO_x conditions, the SOA components are acidic and form upon the further oxidation of MACR. SOA components formed under low- NO_x conditions, by contrast, are not acidic, with primary species identified being polyols and organic peroxides. Based on SOA growth, acid-catalysis seems to play a larger role under low- NO_x conditions. Organic peroxides (likely dominated by hydroperoxides) contribute significantly to the low- NO_x SOA mass ($\sim 61\%$

for nucleation experiments and ~ 25% and 30% for dry seeded and acid seeded experiments, respectively). However, differences in the organic peroxide contribution and the rate of loss in SOA mass for nucleation (seed-free) and seeded experiments are not well understood and require further investigation. The chemical composition changes with time in the low-NO_x case, showing evidence of chemical aging.

Oligomerization is an important SOA formation pathway for both low- and high-NO_x conditions, as oligomers were observed in both cases. The nature of the oligomers, however, is distinctly different in each NO_x regime. Under high-NO_x conditions, the oligomers have clear monomeric units, with observable 102 Da differences using both online and offline mass spectrometry techniques. Using tandem ESI-MS techniques and GC/MS with trimethylsilylation, it is found that polyesters account for these high-NO_x oligomers, with 2-MG as the key monomeric unit. These polyesters account only for a fraction (~ 22–34%) of the SOA mass formed from isoprene oxidation. This lack of mass closure could result from an underestimate of the amount of polyesters formed or additional, unidentified MACR or isoprene oxidation products that contribute to the SOA mass. One key unresolved question is the path by which 2-MG is formed, which at present is not understood. Further gas- and particle-phase studies on isoprene oxidation under high-NO_x conditions are needed in order to elucidate the 2-MG formation pathway.

Previously detected tracer compounds for isoprene oxidation in the ambient atmosphere were detected in the low-NO_x experiments. C₅ alkene triols and hemiacetal dimers are reported here for the first time in a controlled laboratory experiment, suggesting that the oxidative conditions used in these experiments are relevant to remote regions. The GC/MS results suggest that hemiacetal dimers formed in these low-NO_x

chamber experiments result from the reactions of 2-methyltetrols and C₅ alkene triols (a reaction that is likely relevant to the real atmosphere). Besides the formation of hemiacetal (acetal) oligomers in low-NO_x SOA, it is speculated that peroxyhemiacetal oligomers could also form, due to the large amounts of peroxides measured in the particle phase. The formation of low-NO_x oligomers may correlate to the decomposition of peroxides with experimental time, providing some insight into the mechanism of oligomerization. Additional analytical techniques need to be developed in order to elucidate the neutral/unstable products found in SOA produced from the photooxidation of isoprene.

2.7 Acknowledgements

Research at Caltech was funded by the U.S. Environmental Protection Agency to Achieve Results (STAR) Program grant number RD-83107501-0, managed by EPA's Office of Research and Development (ORD), National Center for Environmental Research (NCER), and by the U.S. Department of Energy, Biological, and Environmental Research Program DE-FG02-05ER63983; this work has not been subjected to the EPA's required peer and policy review and therefore does not necessarily reflect the views of the Agency and no official endorsement should be inferred. Jason Surratt was supported in part by the United States Environmental Protection Agency (EPA) under the Science to Achieve Results (STAR) Graduate Fellowship Program. Research at the Universities of Antwerp and Ghent was supported by the Belgian Federal Science Policy Office through the BIOSOL project (contract SD/AT/02A) and a visiting postdoctoral fellowship to Rafal Szmigielski, and by the Research Foundation – Flanders (FWO). We would like to thank John Greaves at the University of California, Irvine for the accurate mass

measurements on the ESI-TOF instrument. We would like to also thank Paul Ziemann at the University of California, Riverside for his useful communications regarding peroxide measurements in SOA.

2.8 References

- (1) Iinuma, Y.; Böge, O.; Gnauk, T.; Herrmann, H. *Atmos. Environ.* **2004**, *38*, 761.
- (2) Gao, S.; Keywood, M.; Ng, N.; Surratt, J. D.; Varutbangkul, V.; Bahreini, R.; Flagan, R. C.; Seinfeld, J. H. *J. Phys. Chem. A* **2004**, *108*, 10147.
- (3) Gao, S.; Ng, N.; Keywood, M.; Varutbangkul, V.; Bahreini, R.; Nenes, A.; He, J.; Yoo, K.; Beauchamp, J.; Hodyss, R.; Flagan, R.; Seinfeld, J. *Environ. Sci. Technol.* **2004**, *38*, 6582.
- (4) Tolocka, M.; Jang, M.; Ginter, J.; Cox, F.; Kamens, R.; Johnston, M. *Environ. Sci. Technol.* **2004**, *38*, 1428.
- (5) Kalberer, M.; Paulsen, D.; Sax, M.; Steinbacher, M.; Dommen, J.; Prevot, A.; Fisseha, R.; Weingartner, E.; Frankevich, V.; Zenobi, R.; Baltensperger, U. *Science* **2004**, *303*, 1659.
- (6) Kanakidou, M.; Seinfeld, J.; Pandis, S.; Barnes, I.; Dentener, F.; Facchini, M.; Van Dingenen, R.; Ervens, B.; Nenes, A.; Nielsen, C.; Swietlicki, E.; Putaud, J.; Balkanski, Y.; Fuzzi, S.; Horth, J.; Moortgat, G.; Winterhalter, R.; Myhre, C.; Tsigaridis, K.; Vignati, E.; Stephanou, E.; Wilson, J. *Atmos. Chem. Phys.* **2005**, *5*, 1053.
- (7) Claeys, M.; Graham, B.; Vas, G.; Wang, W.; Vermeylen, R.; Pashynska, V.; Cafmeyer, J.; Guyon, P.; Andreae, M. O.; Artaxo, P.; Maenhaut, W. *Science* **2004**, *303*, 1173.
- (8) Pandis, S.; Paulson, S.; Seinfeld, J. H.; Flagan, R. C. *Atmos. Environ.* **1991**, *25*, 997.
- (9) Limbeck, A.; Kulmala, M.; Puxbaum, H. *Geophys. Res. Lett.* **2003**, *30*.
- (10) Ion, A. C.; Vermeylen, R.; Kourtchev, I.; Cafmeyer, J.; Chi, X.; Gelencsér, A.; Maenhaut, W.; Claeys, M. *Atmos. Chem. Phys.* **2005**, *5*, 1805.
- (11) Kourtchev, I.; Ruuskanen, T.; Maenhaut, W.; Kulmala, M.; Claeys, M. *Atmos. Chem. Phys.* **2005**, *5*, 2761.
- (12) Wang, W.; Kourtchev, I.; Graham, B.; Cafmeyer, J.; Maenhaut, W.; Claeys, M. *Rapid Commun. Mass Spectrom.* **2005**, *19*, 1343.

- (13) Claeys, M.; Wang, W.; Ion, A.; Kourtchev, I.; Gelencsér, A.; Maenhaut, W. *Atmos. Environ.* **2004**, *38*, 4093.
- (14) Edney, E. O.; Kleindienst, T. E.; Jaoui, M.; Lewandowski, M.; Offenbergh, J. H.; Wang, W.; Claeys, M. *Atmos. Environ.* **2005**, *39*, 5281.
- (15) Böge, O.; Miao, Y.; Plewka, A.; Herrmann, H. *Atmos. Environ.* **2006**, *40*, 2501.
- (16) Kroll, J.; Ng, N. L.; Murphy, S. M.; Flagan, R. C.; Seinfeld, J. H. *Geophys. Res. Lett.* **2005**, *32*.
- (17) Kroll, J. H.; Ng, N. L.; Murphy, S. M.; Flagan, R. C.; Seinfeld, J. H. *Environ. Sci. Technol.* **2006**, *40*, 1869.
- (18) Docherty, K.; Wu, W.; Lim, Y.; Ziemann, P. *Environ. Sci. Technol.* **2005**, *39*, 4049.
- (19) Johnson, D.; Jenkin, M. E.; Wirtz, K.; Martin-Reviejo, M. *Environ. Chem.* **2004**, *1*, 150.
- (20) Gao, S.; Surratt, J. D.; Knipping, E. M.; Edgerton, E. S.; Shahgholi, M.; Seinfeld, J. H. *J. Geophys. Res.* **2006**, *in press*.
- (21) Cocker, D.; Flagan, R. C.; Seinfeld, J. H. *Environ. Sci. Technol.* **2001**, *35*, 2594.
- (22) Keywood, M.; Varutbangkul, V.; Bahreini, R.; Flagan, R.; Seinfeld, J. *Environ. Sci. Technol.* **2004**, *38*, 4157.
- (23) Lai, C.; Tsai, C.; Tsai, F.; Lee, C.; Lin, W. *Rapid Commun. Mass Spectrom.* **2001**, *15*, 2145.
- (24) Drewnick, F.; Hings, S.; DeCarlo, P.; Jayne, J.; Gonin, M.; Fuhrer, K.; Weimer, S.; Jimenez, J.; Demerjian, K.; Borrmann, S.; Worsnop, D. *Aerosol Sci. Technol.* **2005**, *39*, 637.
- (25) Pashynska, V.; Vermeylen, R.; Vas, G.; Maenhaut, W.; Claeys, M. *J. Mass Spectrom.* **2002**, *37*, 1249.
- (26) Banerjee, D.; Budke, C. *Anal. Chem.* **1964**, *36*, 792.
- (27) Sorooshian, A.; Brechtel, F. J.; Ma, Y.; Weber, R. J.; Corless, A.; Flagan, R. C.; Seinfeld, J. H. *Aerosol Sci. Technol.* **2006**, *in press*.
- (28) Weber, R.; Orsini, D.; Daun, Y.; Lee, Y.; Klotz, P.; Brechtel, F. *Aerosol Sci. Technol.* **2001**, *35*, 718.

- (29) Seinfeld, J. H.; Pandis, S. N. *Atmospheric Chemistry and Physics: From Air Pollution to Climate Change*; Wiley: New York, 1998.
- (30) Iinuma, Y.; Böge, O.; Miao, Y.; Sierau, B.; Gnauk, T.; Herrmann, H. *Faraday Discuss.* **2005**, *130*, 279.
- (31) Knochenmuss, R.; Zenobi, R. *Chem. Rev.* **2003**, *103*, 441.
- (32) Miyoshi, A.; Hatakeyama, S.; Washida, N. *J. Geophys. Res.* **1994**, *99*, 18779.
- (33) Tuazon, E.; Atkinson, R. *Int. J. Chem. Kinet.* **1990**, *22*, 1221.
- (34) Paulson, S.; Flagan, R. C.; Seinfeld, J. H. *Int. J. Chem. Kinet.* **1992**, *24*, 79.
- (35) Sprengnether, M.; Demerjian, K.; Donahue, N.; Anderson, J. *J. Geophys. Res.* **2002**, *107*.
- (36) Baker, J.; Arey, J.; Atkinson, R. *Environ. Sci. Technol.* **2005**, *39*, 4091.
- (37) Ng, N. L.; Kroll, J. H.; Keywood, M. D.; Bahreini, R.; Varutbangkul, V.; Lee, A.; Goldstein, A. H.; Flagan, R. C.; Seinfeld, J. H. *Environ. Sci. Technol.* **2006**, *40*, 2283.
- (38) Lee, A.; Goldstein, A. H.; Ng, N. L.; Kroll, J. H.; Varutbangkul, V.; Flagan, R. C.; Seinfeld, J. H. *J. Geophys. Res.* **2006**, *111*.
- (39) Chuong, B.; Stevens, P. S. *Int. J. Chem. Kinet.* **2004**, *36*, 12.
- (40) Yuan, H.; Nishiyama, Y.; Kuga, S. *Cellulose* **2005**, *12*, 543.
- (41) Kroll, J. H.; Ng, N. L.; Murphy, S. M.; Varutbangkul, V.; Flagan, R. C.; Seinfeld, J. H. *J. Geophys. Res.* **2005**, *110*.
- (42) Liggio, J.; Li, S.; McLaren, R. *Environ. Sci. Technol.* **2005**, *39*, 1532.
- (43) Barsanti, K.; Pankow, J. *Atmos. Environ.* **2005**, *39*, 6597.
- (44) Tong, C.; Blanco, M.; Goddard III, W. A.; Seinfeld, J. H. *Environ. Sci. Technol.* **2006**, *40*, 2333.
- (45) Johnson, D.; Jenkin, M. E.; Wirtz, K.; Martin-Reviejo, M. *Environ. Chem.* **2005**, *2*, 35.
- (46) Bonn, B.; von Kuhlmann, R.; Lawrence, M. *Geophys. Res. Lett.* **2004**, *31*.
- (47) Decesari, S.; Fuzzi, S.; Facchini, M.; Mircea, M.; Emblico, L.; Cavalli, F.;

Maenhaut, W.; Chi, X.; Schkolnik, G.; Falkovich, A.; Rudich, Y.; Claeys, M.; Pashynska, V.; Vas, G.; Kourtchev, I.; Vermeylen, R.; Hoffer, A.; Andreae, M. O.; Tagliavini, E.; Moretti, F.; Artaxo, P. *Atmos. Chem. Phys.* **2006**, *6*, 375.

Table 2.1. High-NO_x chamber experiments conducted.

| expt. no. | VOC ^a | OH precursor ^b | seeded ^c / nucleation | initial [NO] ppb | initial [NO ₂] ppb | initial [NO _x] ppb | [O ₃] ^d ppb | T, °C ^d | total SOA mass concentration ^{d,e,f} μg/m ³ |
|----------------|------------------|-------------------------------|-------------------------------------|---------------------|--------------------------------------|--------------------------------------|---------------------------------------|--------------------|---|
| 1 | Isoprene | H ₂ O ₂ | nucleation | 826.7 | 33.9 | 859.5 | 497.7 | 28.5 | 74 |
| 2 | Isoprene | H ₂ O ₂ | dry AS | 758.5 | 112.0 | 868.9 | 525.3 | 28.3 | 73 |
| 3 | MACR | H ₂ O ₂ | dry AS | 791.4 | 60.0 | 850.3 | 539.7 | 25.2 | 181 |
| 4 | MACR | H ₂ O ₂ | nucleation | 897.7 | 29.8 | 926.2 | 519.0 | 25.0 | 197 |
| 5 | Isoprene | H ₂ O ₂ | nucleation | 805.5 | 87.3 | 891.2 | 294.2 | 24.3 | 104 |
| 6 | Isoprene | H ₂ O ₂ | AAS | 825.1 | 80.4 | 904.1 | 450.0 | 24.6 | 111 |
| 7 ^g | Isoprene | HONO | dry AS | 50.0 | 332.5 | 381.5 | 131.7 | 20.1 | 68 |
| 8 ^g | Isoprene | HONO | nucleation | 89.1 | 278.7 | 366.3 | 134.4 | 21.4 | 73 |
| 9 | Isoprene | H ₂ O ₂ | dry AS | 891.2 | 73.6 | 963.1 | 325.4 | 24.9 | 95 |

^aAll VOC gas phase concentrations were 500 ppb. MACR = methacrolein.

^bH₂O₂ and HONO are not measured directly, but from isoprene decay during irradiation we estimate ~ 3ppm of H₂O₂ and HONO is unlikely greater than measured [NO₂].

^cAS = ammonium sulfate seed, AAS = acidic ammonium sulfate seed

^dAverged over the course of the filter sampling.

^eSubtraction of seed aerosol taken into account when necessary. SOA volume derived from DMA wall loss uncorrected measurements.

^fAssuming an SOA density of 1.35 g/cm³. This is derived from comparison of DMA aerosol volume and AMS aerosol mass measurements.

^g10% of light bank used and hence lower temperature observed. Also lower amounts of initial NO due to HONO as precursor.

Table 2.2. Quantified SOA products (in ng m⁻³) from High-NO_x chamber experiments.

| | [M-H] ⁻ ion | Surrogate Standard Used for Quantification ^a | Isoprene/High NO _x /H ₂ O ₂ | | | | MACR/High NO _x /H ₂ O ₂ | | Isoprene/HONO | |
|---|------------------------|---|--|--------|---------|--------|--|---------|---------------|---------|
| | | | Exp 1 | Exp 2 | Exp 6 | Exp 9 | Exp 3 | Exp 4 | Exp 7 | Exp 8 |
| mono - nitrate oligomers | 266 | pimelic acid | 1966.0 | 4164.9 | 3886.3 | 3907.3 | 9354.7 | 3859.8 | 1474.3 | 830.0 |
| | 368 | pinic acid | 1350.3 | 2454.2 | 3704.9 | 4442.1 | 20619.7 | 10078.8 | 834.7 | 752.3 |
| | 470 | pinic acid | 2329.5 | 2931.5 | 2298.5 | 2640.0 | 28897.5 | 16679.6 | | 208.2 |
| | 572 | pinic acid | | | | | 2956.6 | 6810.4 | | |
| | 674 | suberic acid monomethyl ester | | | | | 918.9 | 705.1 | | |
| | 776 | suberic acid monomethyl ester | | | | | 664.7 | 453.7 | | |
| | 878 | suberic acid monomethyl ester | | | | | 216.1 | 211.8 | | |
| Total mass from <i>mono</i> -nitrate oligomers (µg/m ³) | | | 5.6 | 9.6 | 9.9 | 11.0 | 63.6 | 38.8 | 2.3 | 1.8 |
| % Contribution to the Total SOA Mass | | | 7.6 | 13.1 | 8.9 | 11.6 | 35.2 | 19.7 | 3.4 | 2.5 |
| 2-MG acid oligomers | 119 | meso-erythritol | 2051.9 | 3173.7 | 9681.6 | 4492.4 | 1236.9 | 458.6 | 4168.1 | 11612.6 |
| | 221 | citramalic acid | 1173.8 | 2589.3 | 2327.6 | 2108.9 | 3841.2 | 1723.6 | 553.0 | 995.9 |
| | 323 | 2-hydroxy-3-methylbutyric acid | 626.6 | 968.6 | 429.9 | 467.5 | 2739.3 | 1320.0 | 70.0 | 156.3 |
| | 425 | pimelic acid | | 282.3 | 286.1 | 255.2 | 1647.2 | 684.1 | | 132.9 |
| | 527 | pimelic acid | | | | | 717.6 | 476.4 | | |
| Total mass from 2-MG acid oligomers (µg/m ³) | | | 3.9 | 7.0 | 12.7 | 7.3 | 10.2 | 4.7 | 4.8 | 12.9 |
| % Contribution to the Total SOA Mass | | | 5.2 | 9.6 | 11.5 | 7.8 | 5.6 | 2.4 | 7.1 | 17.7 |
| mono - acetate oligomers | 161 | citramalic acid | 1.8 | 43.0 | 104.3 | | 87.8 | | 114.1 | 69.5 |
| | 263 | 2-hydroxy-3-methylbutyric acid | 675.8 | 1721.7 | 597.7 | 671.3 | 4066.7 | 1303.9 | 357.2 | 163.5 |
| | 365 | pimelic acid | 769.1 | 1884.7 | 823.2 | 1240.0 | 4824.5 | 1760.3 | 253.0 | 292.6 |
| | 467 | pinic acid | 337.5 | 447.4 | 184.2 | 416.6 | 3748.0 | 1312.7 | | 133.1 |
| | 569 | pinic acid | | 794.4 | | | 8598.9 | 2960.9 | | |
| | 671 | suberic acid monomethyl ester | | | | | 453.8 | 359.4 | | |
| Total mass from <i>mono</i> -acetate oligomers (µg/m ³) | | | 1.8 | 4.9 | 1.7 | 2.3 | 21.8 | 7.7 | 0.7 | 0.7 |
| % Contribution to the Total SOA Mass | | | 2.4 | 6.7 | 1.5 | 2.5 | 12.0 | 3.9 | 1.1 | 0.9 |
| mono - formate oligomers | 147 | meso-erythritol | 202.4 | 375.1 | 11343.4 | | 201.4 | | | 1370.9 |
| | 249 | 2-hydroxy-3-methylbutyric acid | 455.0 | 1339.3 | | 40.1 | 1972.0 | 805.4 | 67.5 | |
| | 351 | 2-hydroxy-3-methylbutyric acid | 367.0 | 997.3 | | 62.0 | 2883.4 | 1386.5 | 33.8 | |
| | 453 | pimelic acid | 290.3 | 378.3 | | | 1795.6 | 711.4 | | |
| Total mass from <i>mono</i> -formate oligomers (µg/m ³) | | | 1.3 | 3.1 | 11.3 | 0.1 | 6.9 | 2.9 | 0.1 | 1.4 |
| % Contribution to the Total SOA Mass | | | 1.8 | 4.2 | 10.2 | 0.1 | 3.8 | 1.5 | 0.2 | 1.9 |
| Total Mass Identified (µg/m ³) | | | 12.6 | 24.5 | 35.7 | 20.7 | 102.4 | 54.1 | 7.9 | 16.7 |
| % of SOA Identified | | | 17.0 | 33.7 | 32.2 | 22.0 | 56.6 | 27.4 | 11.7 | 22.9 |

^aSurrogate standards used covered the range of retention times for detected [M-H]⁻ ions. All standards used were within +/- 1.5 minutes of retention times for sample [M-H]⁻ ions.

^bA blank cell indicates the corresponding species was below detection limits.

Table 2.3. Low-NO_x chamber experiments conducted.

| Exp. No. ^a | Seeded ^b / Nucleation | [NO] ^c ppb | [NO ₂] ^c ppb | [NO _x] ^c ppb | [O ₃] ^c ppb | T, °C ^c | RH, % ^c | SOA Volume Growth Observed ^c μm ³ /cm ³ | Total SOA Mass Concentration ^d μg/m ³ | Peroxide Aerosol Mass Concentration μg/m ³ | % Contribution of Peroxides to the SOA Mass Concentration Observed |
|-----------------------|-------------------------------------|-----------------------|-------------------------------------|-------------------------------------|------------------------------------|--------------------|--------------------|---|--|--|--|
| 1 ^e | nucleation | 33.9 | 24.5 | 0.7 | 32.0 | 29.1 | 5.4 | 148.5 | 185.6 | 116.0 | 62.5 |
| 2 ^e | dry AS | 38.2 | 29.8 | 5.7 | 35.5 | 28.7 | 8.7 | 225.5 | 281.9 | 97.2 | 34.5 |
| 3 | AAS | b.d.l. | 9.5 | 9.4 | b.d.l. | 23.8 | 4.2 | 207.2 | 259.0 | 66.8 | 25.8 |
| 4 | dry AS | b.d.l. | 20.0 | 19.3 | 11.1 | 23.9 | 24.9 | 58.3 | 72.8 | 18.5 | 25.4 |
| 5 ^f | AAS | b.d.l. | 19.4 | 18.8 | b.d.l. | 23.6 | 3.3 | 74.5 | 93.1 | 22.6 | 24.3 |
| 6 | nucleation | b.d.l. | 55.5 | 53.2 | 7.1 | 26.2 | 1.7 | 43.9 | 54.9 | 32.4 | 59.0 |
| 6 ^g | nucleation | b.d.l. | 54.9 | 52.2 | 37.4 | 27.0 | 12.9 | 17.2 | 21.5 | 5.5 | 25.7 |

^a H₂O₂ was the OH precursor used for each low NO_x isoprene experiment. H₂O₂ is not measured directly, but from isoprene decay during irradiation we estimate ~ 3ppm of H₂O₂.

^b AS = ammonium sulfate seed, AAS = acidic ammonium sulfate seed.

^c Averaged over the course of filter sampling.

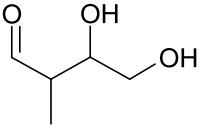
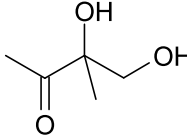
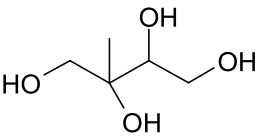
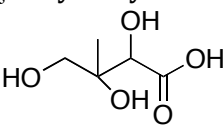
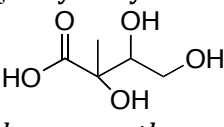
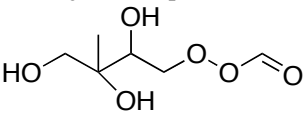
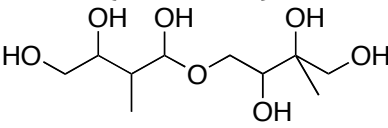
^d Assuming an SOA density of 1.25 g/cm³. This was based on DMA and TOF-AMS measurements.

^e 100% of light bank used and hence higher temperatures in chamber observed during sampling.

^f 100ppb Isoprene experiment.

^g Late sampling, after peak growth, during the aerosol volume growth decay typical of low NO_x experiments.

Table 2.4. Low-NO_x isoprene SOA products elucidated by GC/MS.

| Compound / Structure | MW (MW TMS- derivative) | Elemental composition | Detection in Ambient Atmospheres |
|--|-------------------------------|--|---|
| C₅ alkene triols / ald form  | 118 (334) | C ₅ H ₁₀ O ₃ | [Wang et al., 2005] ¹² [Kourtchev et al., 2005] ¹¹ |
| C₅ alkene triols / keto form  | 118 (334) | C ₅ H ₁₀ O ₃ | [Wang et al., 2005] ¹² [Kourtchev et al., 2005] ¹¹ |
| 2-methyltetrols  <i>threo</i> + <i>erythro</i> | 136 (424) | C ₅ H ₁₂ O ₄ | [Claeys et al., 2004] ⁷ [Edney et al., 2005] ¹⁴ [Böge et al., 2006] ¹⁵ [Ion et al., 2005] ¹⁰ [Kourtchev et al., 2005] ¹¹ |
| C₅ trihydroxy monocarboxylic acid  <i>threo</i> + <i>erythro</i> (minor compounds) | 150 (438) | C ₅ H ₁₀ O ₅ | Not yet detected in ambient aerosol |
| C₅ trihydroxy monocarboxylic acid  <i>threo</i> + <i>erythro</i> (minor compounds) | 150 (438) | C ₅ H ₁₀ O ₅ | Not yet detected in ambient aerosol |
| 2-methyltetrol performate derivatives  (unstable products) | 180 (396) | C ₆ H ₁₂ O ₆ | Not yet detected in ambient aerosol |
| Dimers (6 isomers)  (minor compounds) | 254 (686) | C ₁₀ H ₂₂ O ₇ | Detected in ambient aerosol for the first time in this study |

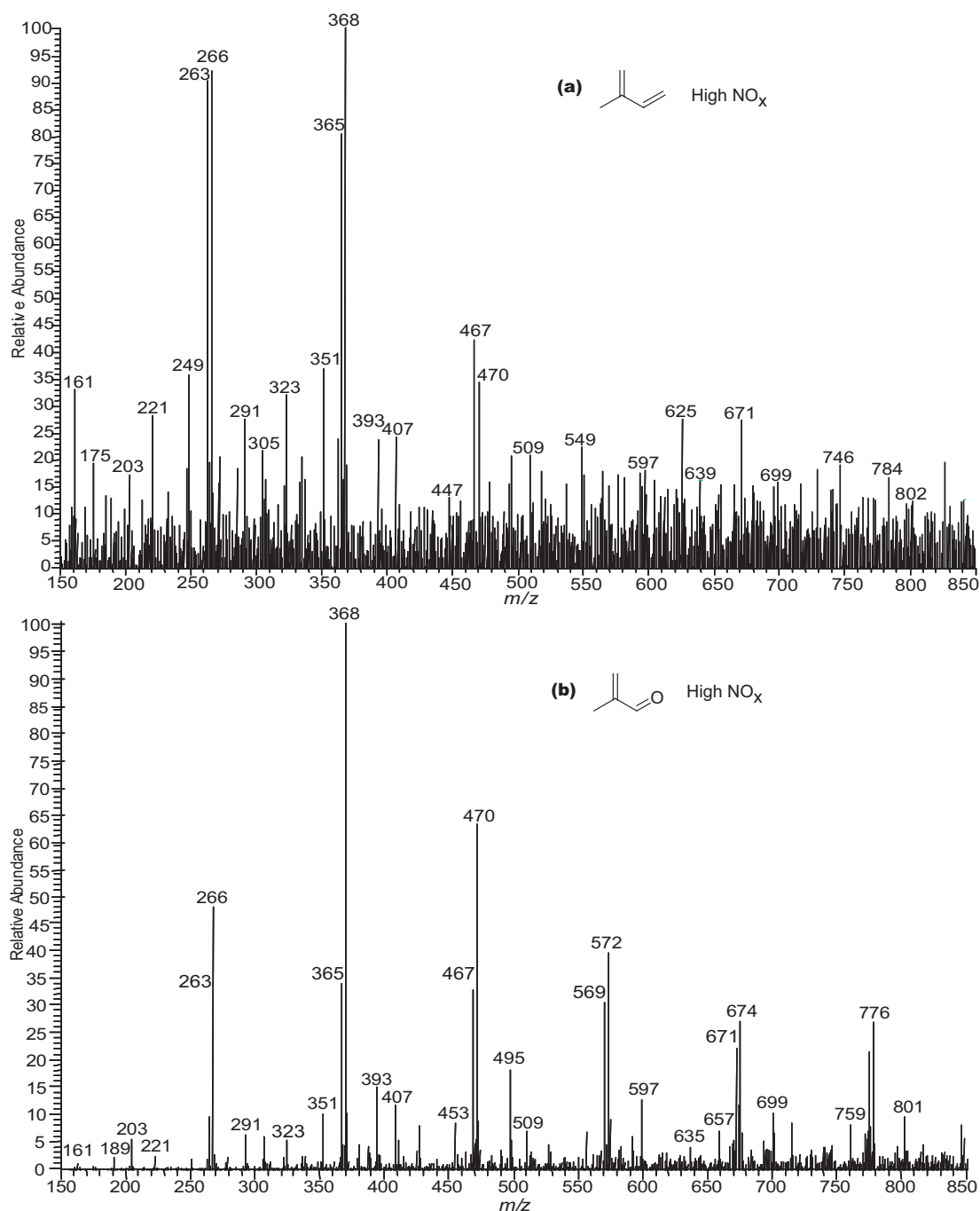


Figure 2.1. ESI-ITMS negative mode spectra collected via direct infusion analyses. (a) MS scan of a filter extract obtained from a 500 ppb isoprene, high- NO_x , seeded experiment. (b) MS scan of a filter extract obtained from a 500 ppb MACR, high- NO_x , seeded experiment. These mass spectra show that MACR oxidation produces many of the same SOA products as that of isoprene oxidation under high- NO_x conditions. Common 102 Da differences between ions in both spectra are observed indicating the presence of oligomers.

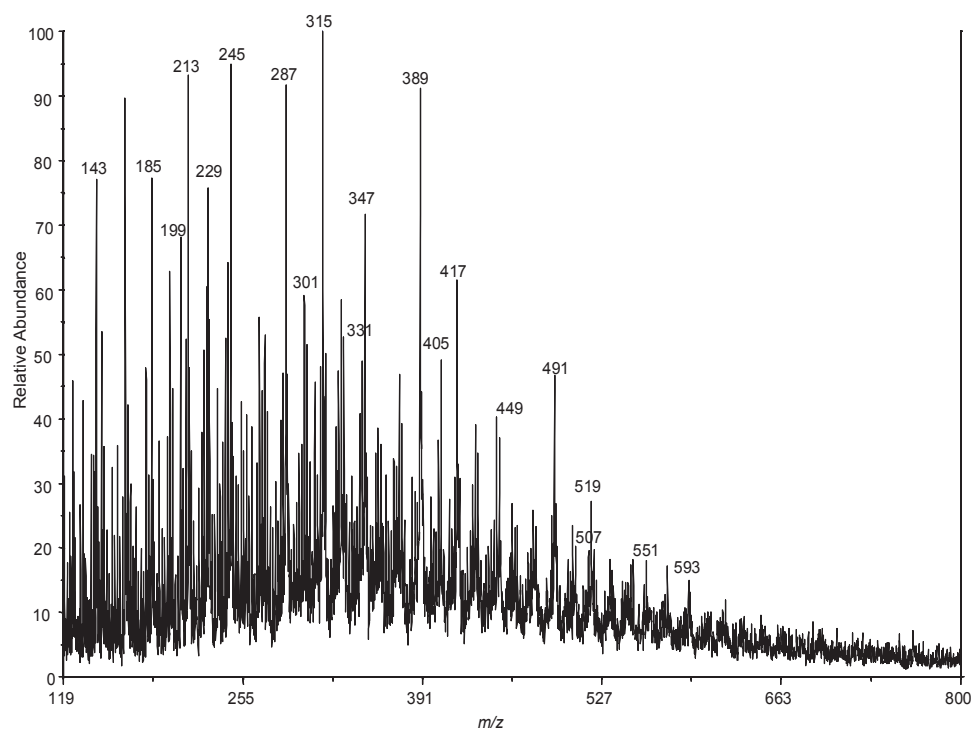


Figure 2.2. MALDI positive mode spectrum obtained with a graphite matrix for a 500 ppb isoprene, high-NO_x, dry seeded experiment (Experiment 9). Highlighted Na⁺ adduct ions confirm the existence of the species detected by ESI.

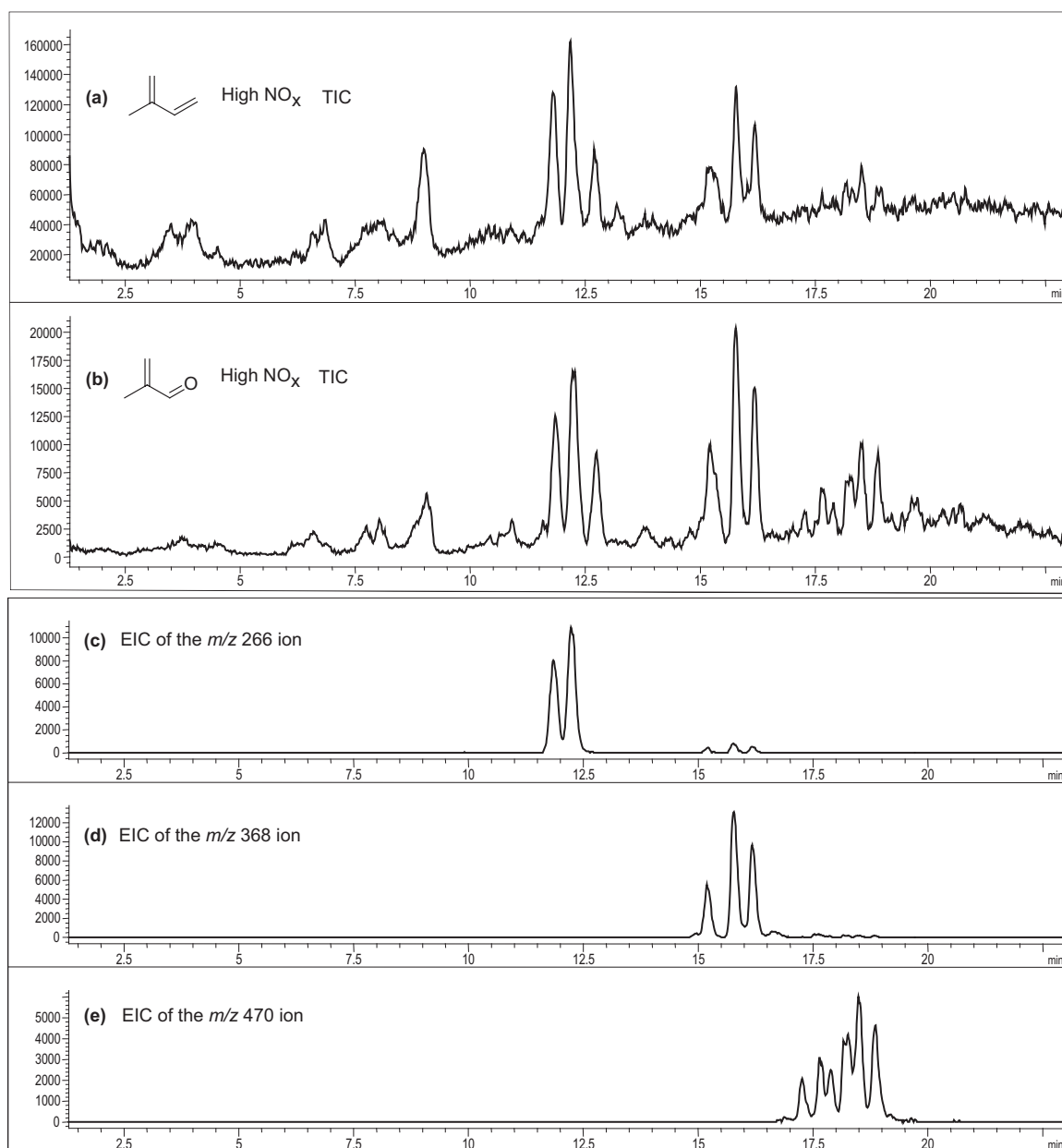


Figure 2.3. (a) LC/MS TIC of a filter extract from a 500 ppb isoprene, high-NO_x, nucleation experiment. (b) LC/MS TIC of a filter extract from a 500 ppb MACR, high-NO_x, nucleation experiment. The similar retention times and mass spectra associated with each chromatographic peak in these two TICs indicate that MACR is an important SOA precursor from isoprene oxidation under high-NO_x conditions. (c), (d), and (e) are LC/MS EICs of organic nitrate species common to both MACR and isoprene high-NO_x samples. These organic nitrate ions are a part of the same oligomeric series confirmed by MS/MS analyses.

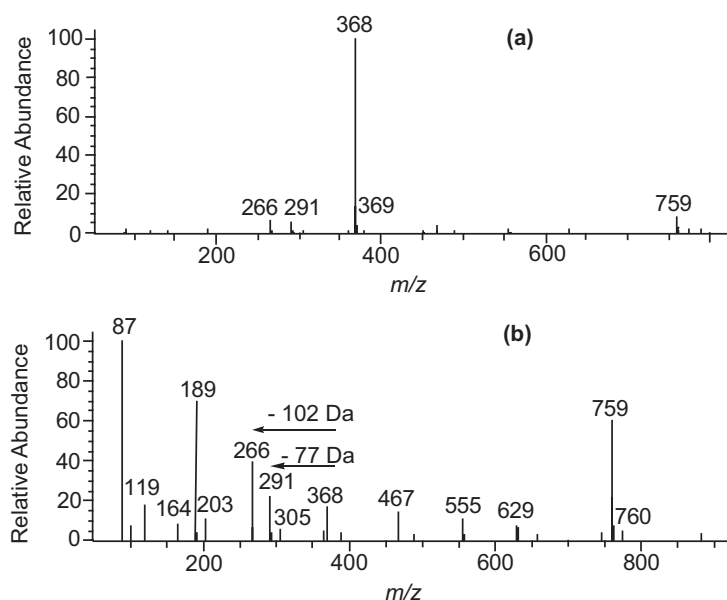


Figure 2.4. (a) Mass spectrum for the largest chromatographic peak (RT = 15.7 min) from Figure 2.3d (EIC of m/z 368 ion). (b) Upfront CID mass spectrum for the same chromatographic peak in Figure 2.3d (EIC of m/z 368 ion). The neutral losses observed in the upfront CID mass spectrum are associated with a trimeric organic nitrate species. This fragmentation pattern of m/z 368 is consistent with ion trap MS/MS results. The product ion m/z 266 corresponds to a neutral loss of 102 Da (common to all MS techniques), the product ion m/z 291 corresponds to a neutral loss of 77 Da (likely CH_3 radical and NO_3 radical, CH_3NO_3), the product ion m/z 305 corresponds to a neutral loss of 63 Da (likely HNO_3), the product ion m/z 203 corresponds to a neutral loss of 165 Da, and the product ion m/z 164 corresponds to a neutral loss of 204 Da (two losses of common monomer).

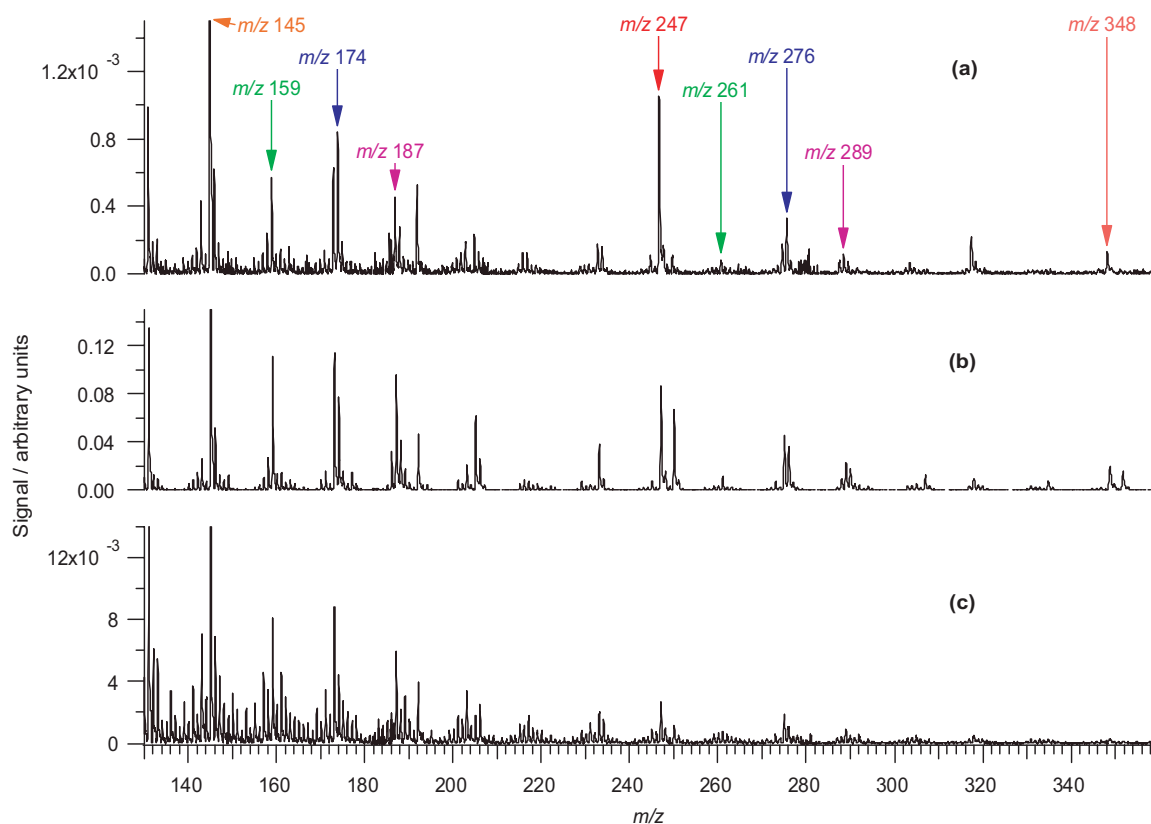


Figure 2.5. TOF-AMS spectra collected at low vaporizer temperatures for the following high- NO_x chamber experiments: (a) 50 ppb isoprene, 250 ppb NO_x , H_2O_2 as the OH precursor, no seed; (b) 500 ppb MACR, 800 ppb NO_x , H_2O_2 as the OH precursor, with seed; and (c) 500 ppb isoprene, HONO as the OH precursor, no seed. These spectra indicate that the OH precursor does not have a substantial effect on the chemistry observed, that MACR is an important SOA precursor from isoprene oxidation, and that the 102 Da differences observed in the offline mass spectrometry data are not a result of sample workup or ionization artifacts.

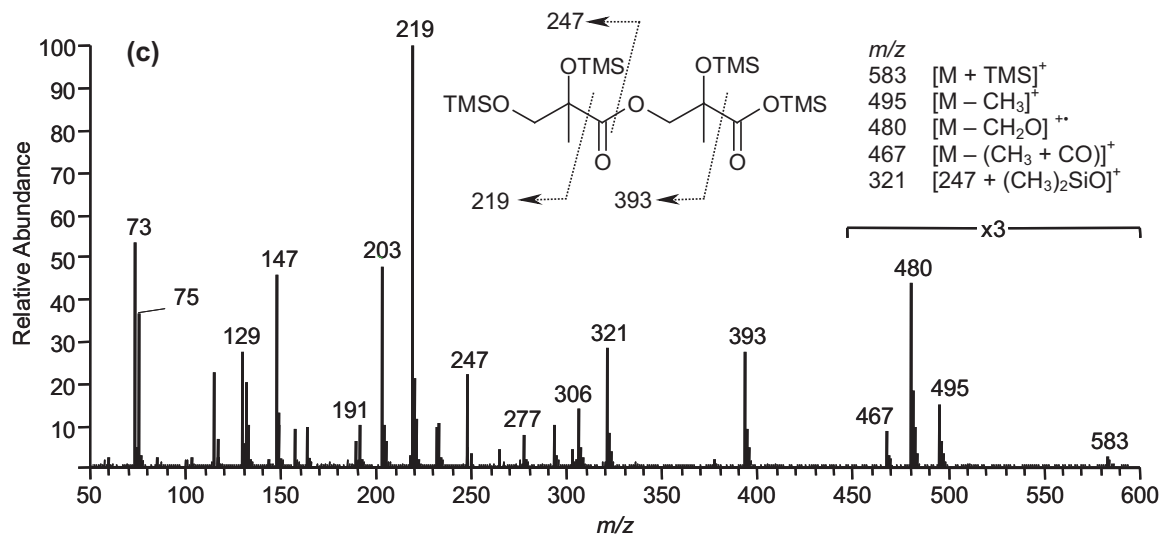
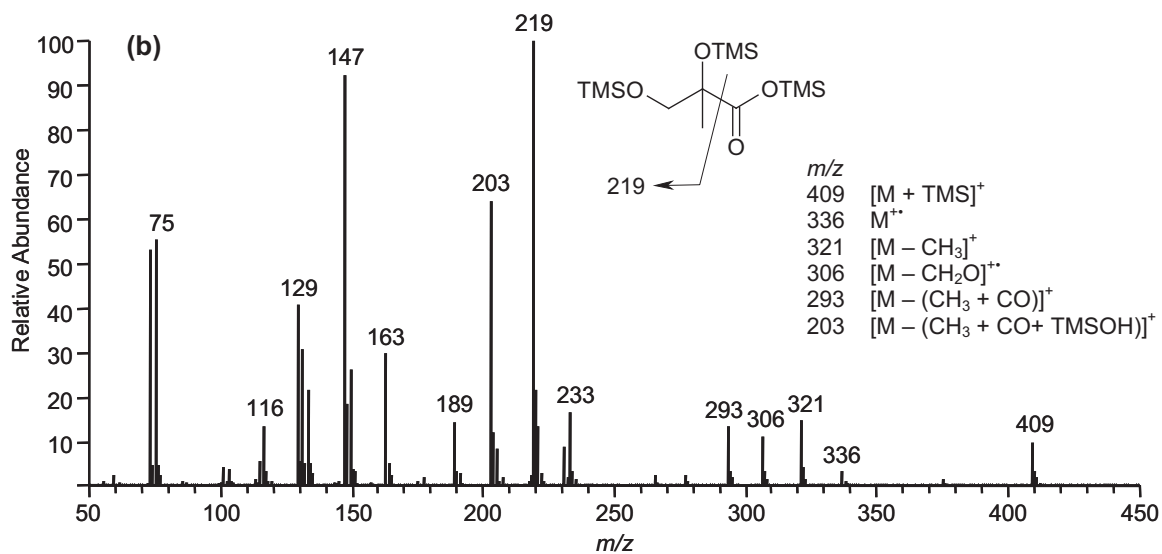
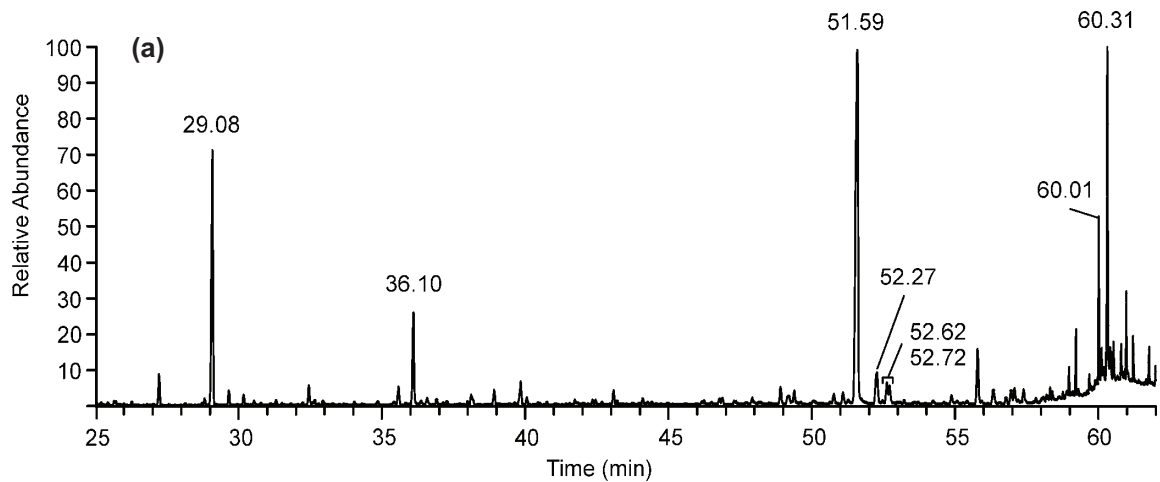


Figure 2.6. (a) TIC of a high-NO_x isoprene nucleation experiment (Experiment 5) collected using GCMS in the EI mode. (b) EI mass spectrum for the 2-MG residue (RT = 29.08 min). (c) EI mass spectrum for a linear dimer made up of two 2-MG residues (RT = 51.59 min). These two mass spectra confirm that 2-MG is present in high-NO_x SOA and that it is involved in particle-phase esterification reactions resulting in polyesters (as shown by the dimer structure above).

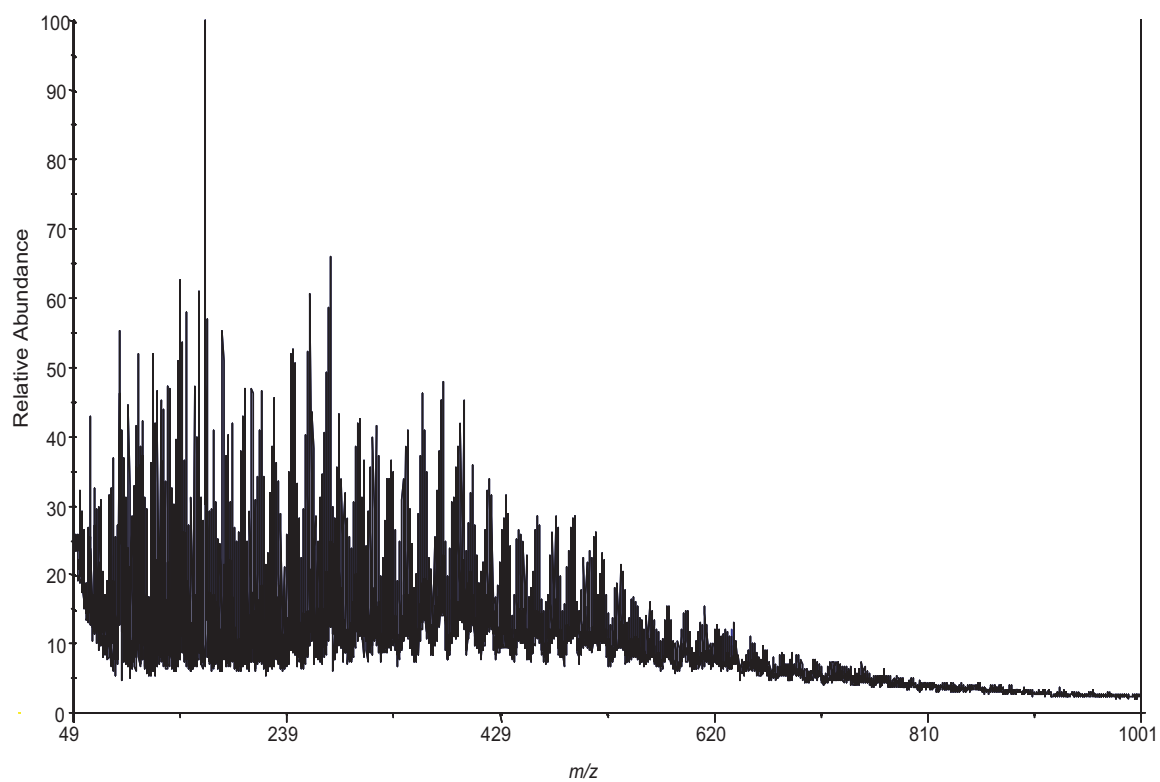


Figure 2.7. MALDI positive mode spectrum obtained with a graphite matrix for a 500 ppb isoprene, low-NO_x, acid seeded experiment (Experiment 14). High-molecular mass species formed up to ~ 620 Da.

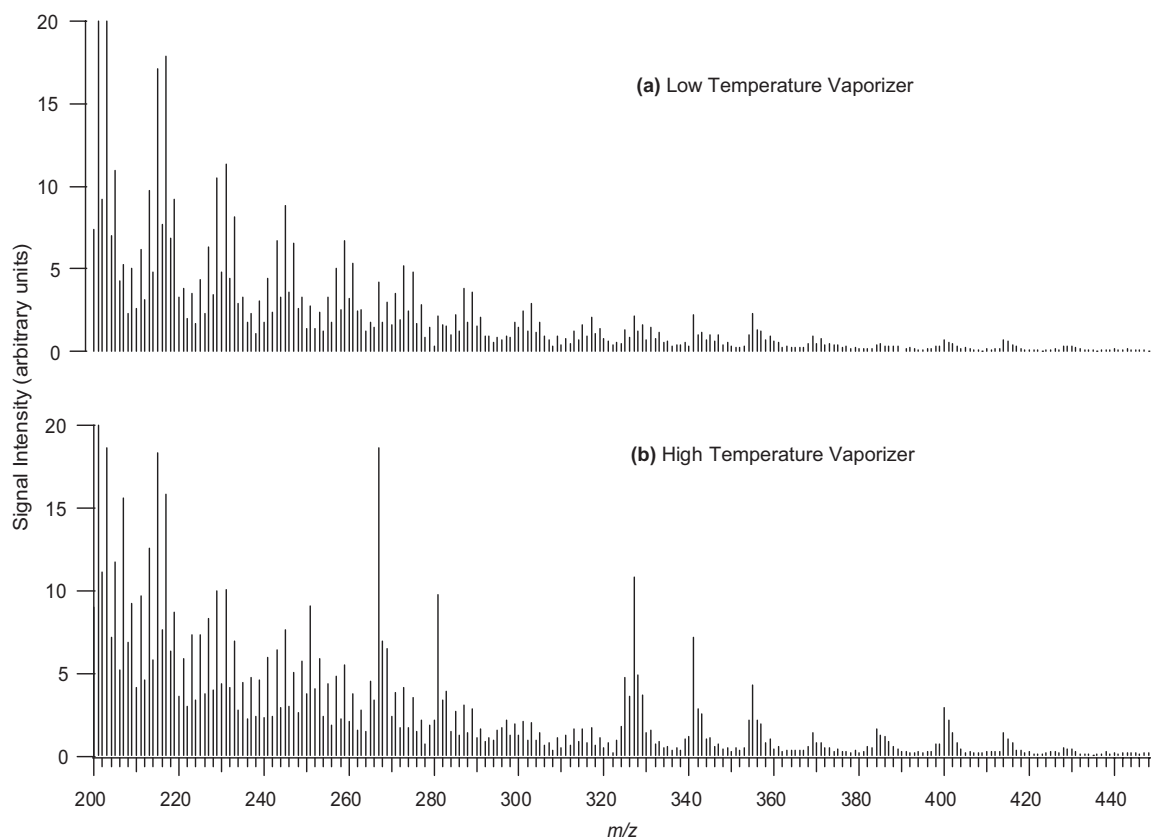


Figure 2.8. TOF-AMS spectra for a 500 ppb isoprene low-NO_x experiment (Experiment 12). (a) Mass spectrum obtained with a low temperature vaporizer (~ 150°C). (b) Mass spectrum obtained with a high temperature vaporizer (~ 600°C). The spectrum is richer at higher temperature with some prominent peaks at higher m/z , indicating that the high-MW oligomers that are not easily volatilized at < 200°C.

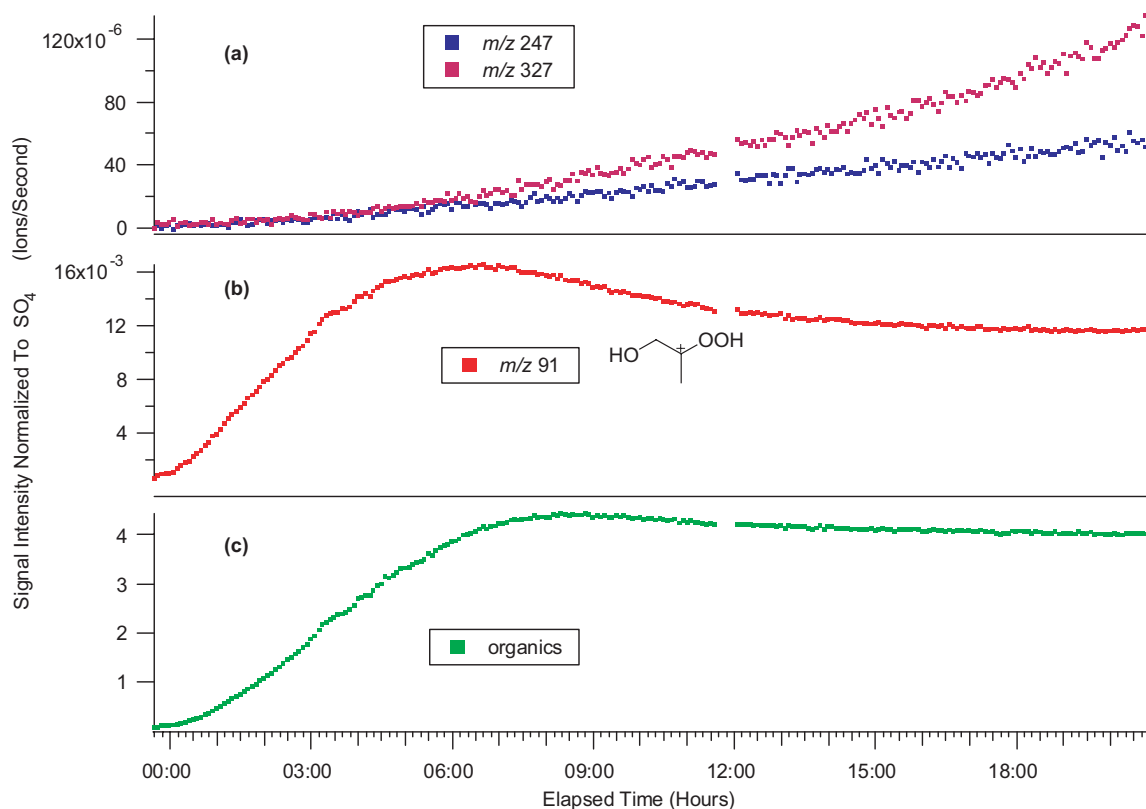


Figure 2.9. Time evolution plots produced from the TOF-AMS instrument for selected fragment ions and the total organic mass observed from a typical low- NO_x experiment (Experiment 13). All ion signal intensities are divided by the signal intensity of sulfate. Because sulfate concentration is a tracer for wall loss (neither created nor removed during the run), the ratio of ion signal to sulfate signal should give an indication of the behavior without wall loss. (a) Time evolution plot for high-mass fragment ions m/z 247 and 327. (b) Time evolution plot for the proposed peroxide fragment ion m/z 91 ($\text{C}_3\text{H}_7\text{O}_3$), where the structure of one isomer is shown. (c) Time evolution plot for the total organic mass. These plots indicate that the chemical composition changes with experimental time, where the decomposition of organic peroxides correlates to oligomerization within low- NO_x SOA. The missing data points (11:30 to 12:00 hours) in these plots are due to the vaporizer in the TOF-AMS instrument being turned off.

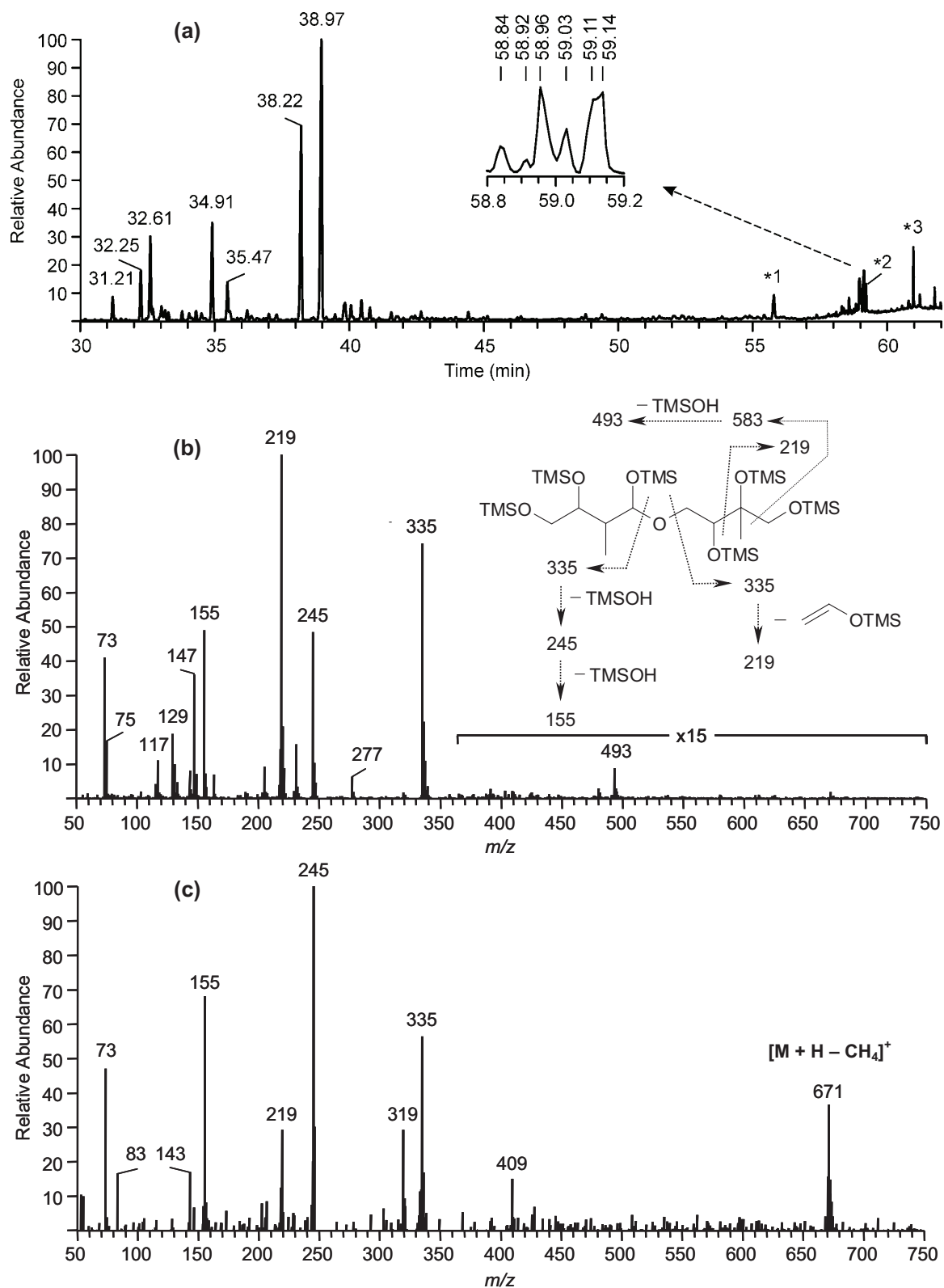


Figure 2.10. (a) GC/MS TIC of isoprene low- NO_x SOA. The insert shows the m/z 219 EIC for the dimeric products eluting between 58.8 and 59.2 min. Peak identifications:

RTs 31.21, 32.25 and 32.61 min: C₅ alkene triols; RTs 34.91 and 35.47 min: unstable products tentatively characterized as 2-methyltetrol performate derivatives; RTs 38.22 and 38.97 min: 2-methyltetrols (2-methylthreitol and 2-methylerythritol, respectively). The EI spectra for the latter seven compounds are provided in Figure 2.20. The peaks labeled *1, *2 and *3 were also present in the laboratory controls and were identified as palmitic acid, stearic acid and palmitoyl monoglyceride, respectively. (b) averaged EI spectrum for the dimeric products eluting between 58.8 and 59.2 min and fragmentation scheme; and (c) averaged CI(CH₄) spectrum for the latter products.

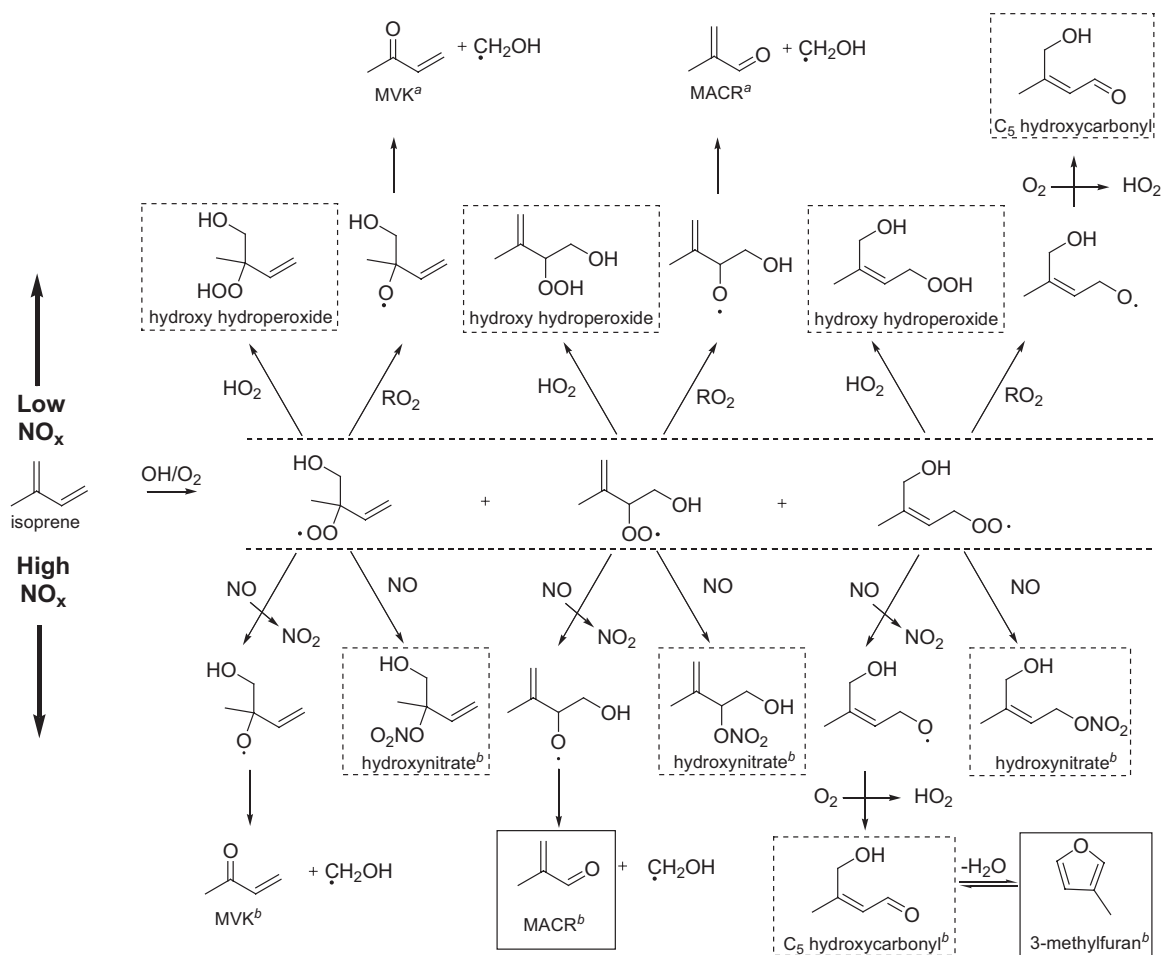


Figure 2.11. Reaction mechanism of isoprene oxidation under low- and high- NO_x conditions. Dotted boxes indicate possible SOA precursors, whereas black boxes indicate known SOA precursors. For simplicity, only three of the eight initial isoprene hydroxyperoxy (RO_2) radicals are shown. $\text{RO}_2 + \text{RO}_2$ reactions leading to diols and other hydroxycarbonyls have been omitted for simplicity. ^aMiyoshi et al.³¹ showed that $[\text{isoprene}]_0/[\text{H}_2\text{O}_2]$ determines molar yields of MVK, MACR, and formaldehyde under low- NO_x conditions. ^bKroll et al.¹⁶ summarized molar yields of gas-phase products from isoprene oxidation under high- NO_x conditions reported in the literature.

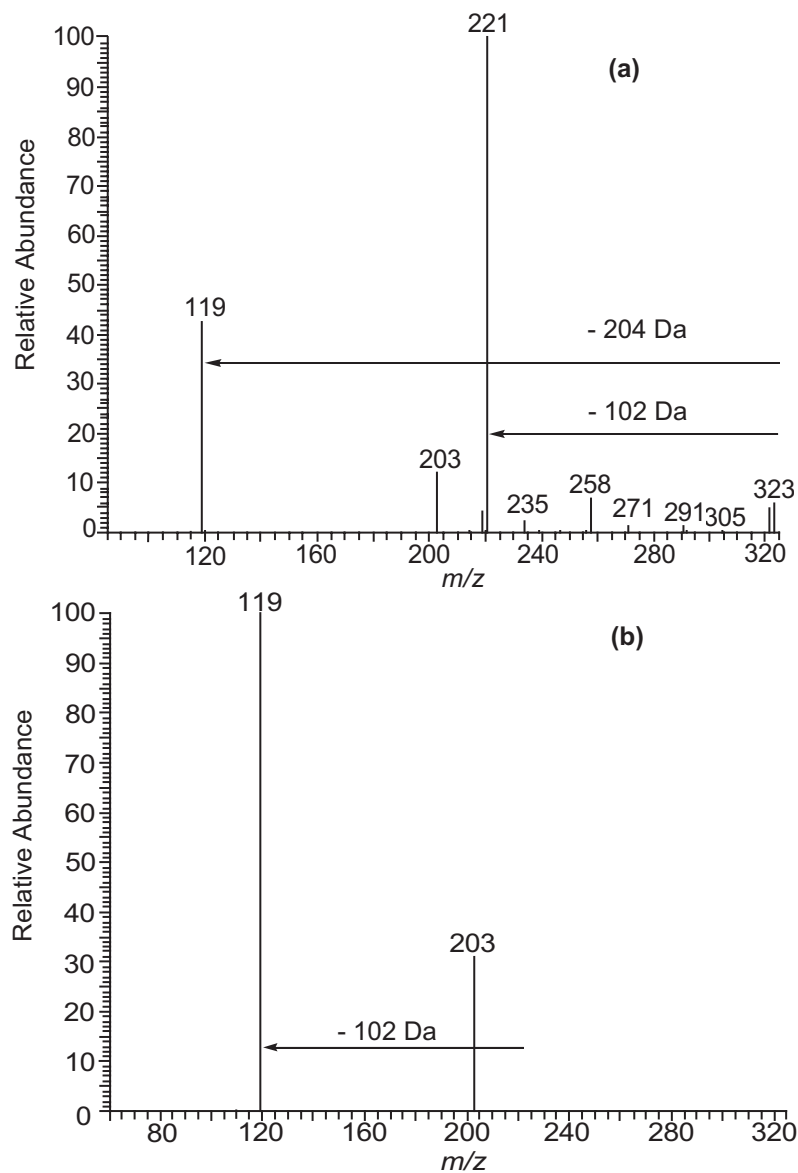


Figure 2.12. ESI-ITMS negative mode product ion spectra from a high- NO_x isoprene SOA sample (Experiment 9). (a) MS^2 spectrum for an isolated m/z 323 ion. Two neutral losses of 102 Da are observed as shown by the product ions m/z 221 and 119. (b) MS^3 spectrum for an isolated m/z 323 ion generated from the further fragmentation of the dominant daughter ion ($= m/z$ 221) in the MS^2 spectrum. These spectra indicate that 2-MG ($[\text{M} - \text{H}]^-$ ion $= m/z$ 119) is a monomer for the oligomeric m/z 323 ion.

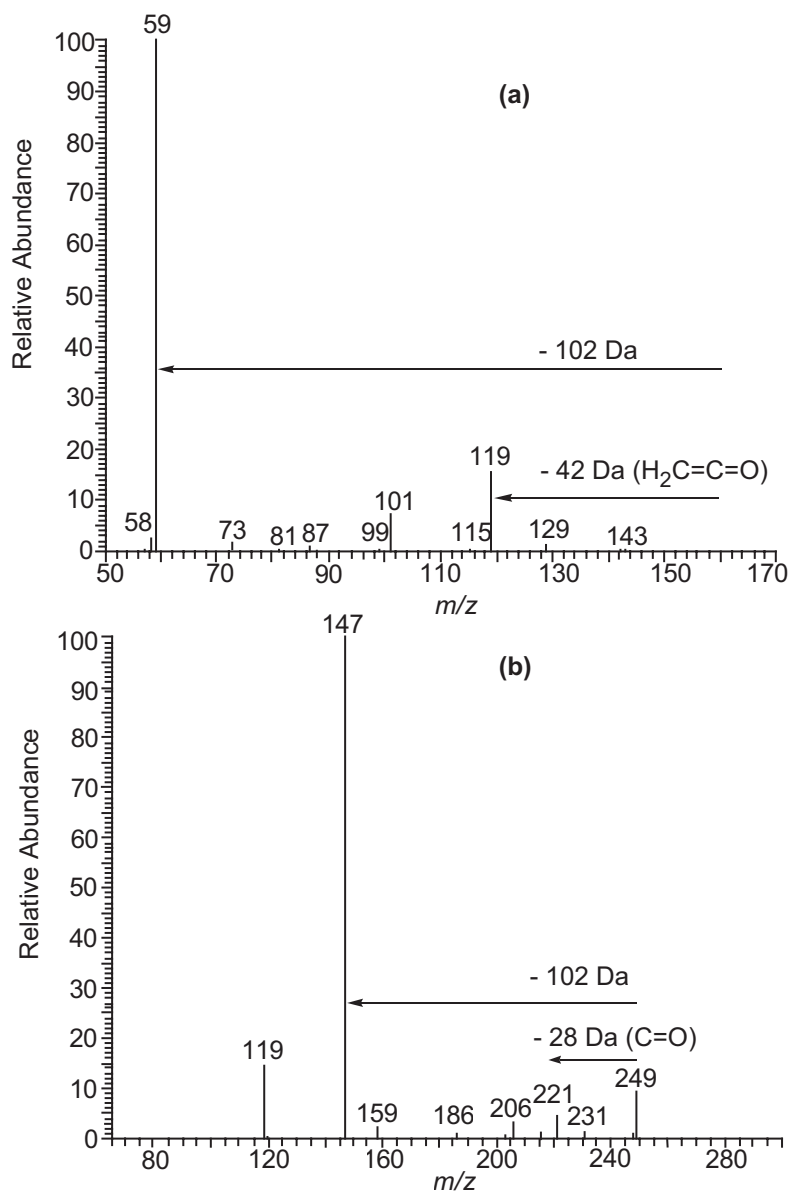


Figure 2.13. ESI-ITMS negative mode product ion mass spectra providing evidence for *mono*-acetate and *mono*-formate oligomers in high- NO_x SOA. (a) Product ion mass spectrum for a *mono*-acetate dimer (m/z 161). (b) Product ion mass spectrum for a *mono*-formate trimer (m/z 249).

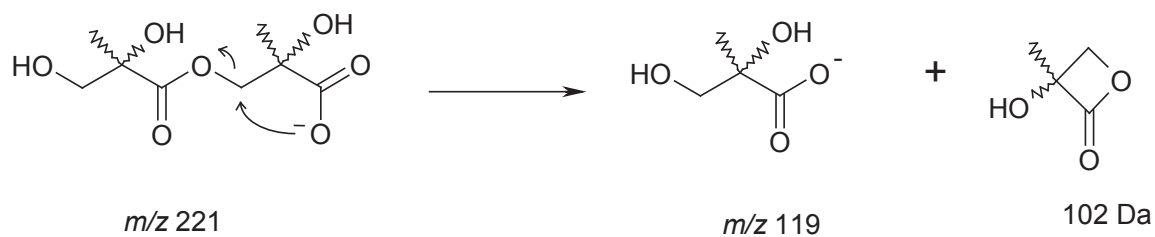


Figure 2.14. Proposed charge-directed nucleophilic reaction occurring during collisional activation in (-)ESI-ITMS, explaining the observation of 102 Da (2-hydroxy-2-methylpropiolactone) losses from oligomeric high-NO_x SOA.

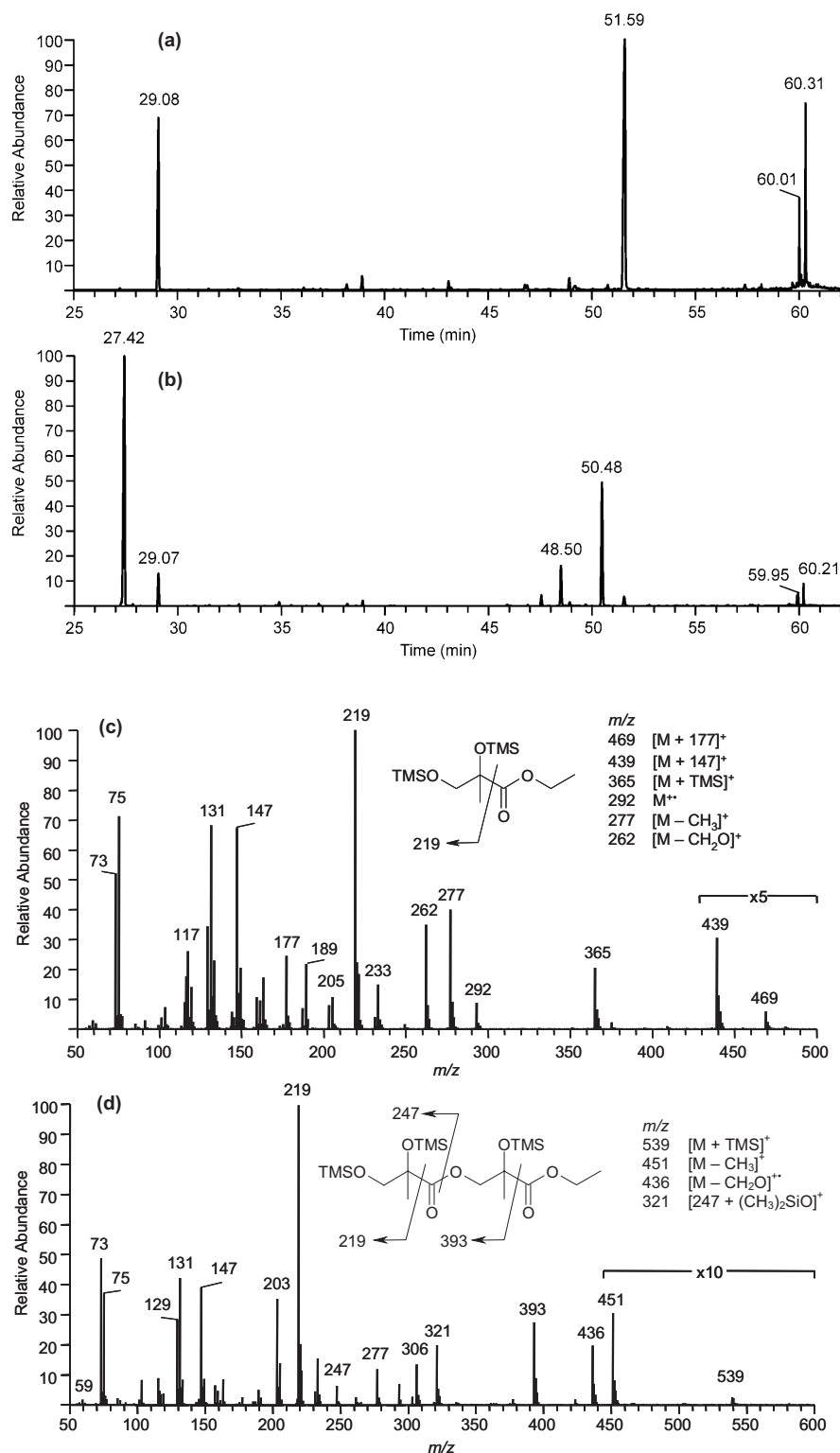


Figure 2.15. (a) GC/MS EIC ($= m/z$ 219) for high- NO_x isoprene nucleation sample (Experiment 5) treated only with TMS derivatization. (b) GC/MS EIC ($= m/z$ 219) for a duplicate sample of same experiment (Experiment 5) in part a, but treated this time by hydrolysis/ethylation followed by TMS derivatization. (c) EI mass spectrum for ethyl ester of 2-MG acid detected in part b (RT = 27.42 min). (d) EI mass spectrum for ethyl

ester of linear 2-MG acid dimer detected in part b (RT =50.48 min). The hydrolysis/ethylation followed by TMS derivatization results presented here confirm the existence of polyesters in high-NO_x SOA.

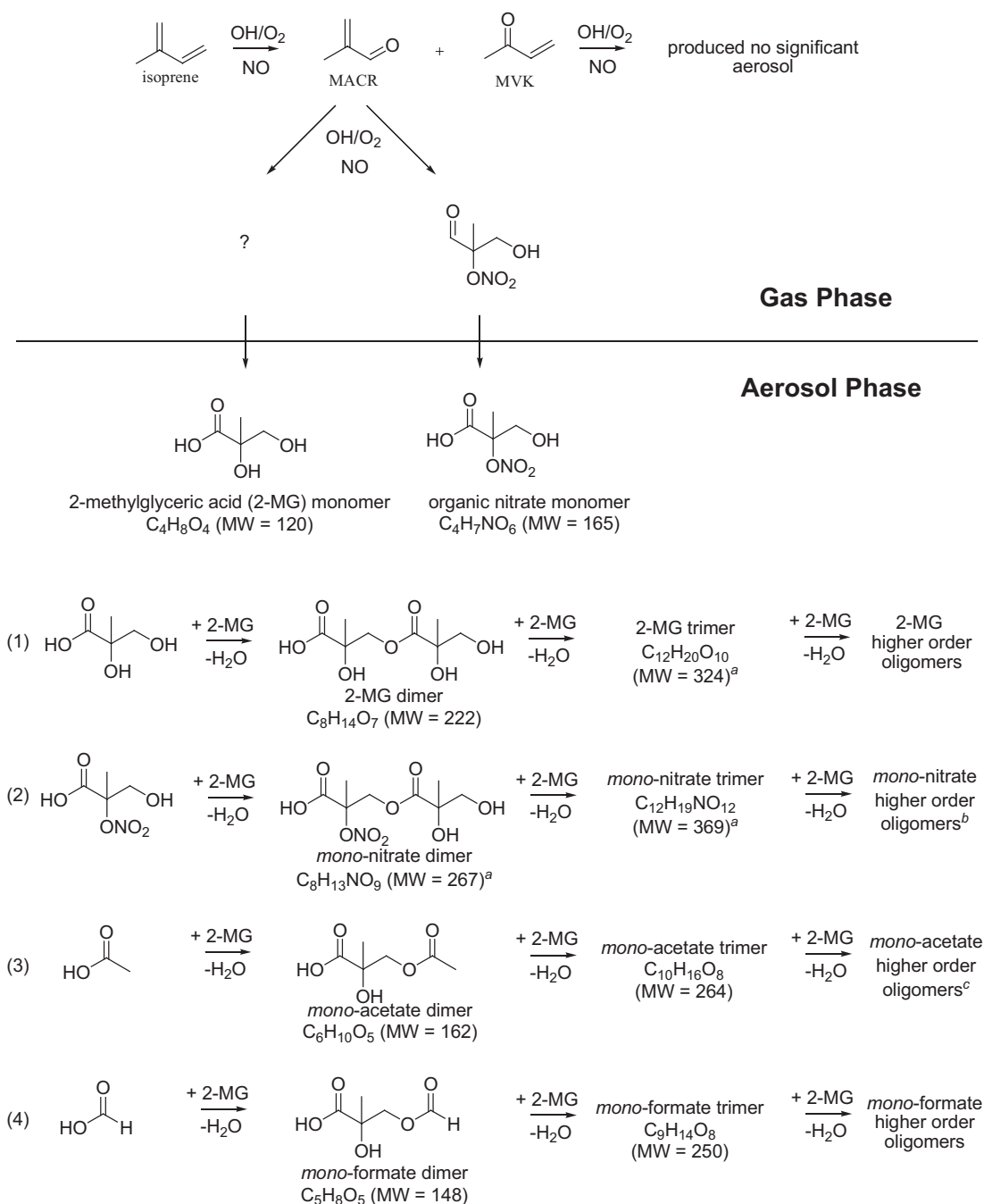


Figure 2.16. Proposed mechanism for SOA formation from isoprene photooxidation under high- NO_x conditions. Symbol used: ?, further study needed in order to understand the formation (in gas/particle phase) of 2-MG. ^aElemental compositions confirmed by high resolution ESI-MS. ^bElemental composition of *mono-nitrate* tetramer (MW = 471) confirmed by high resolution ESI-MS. ^cElemental compositions of *mono-acetate* tetramer and pentamer (MW = 366 and 468, respectively) confirmed by high resolution ESI-MS.

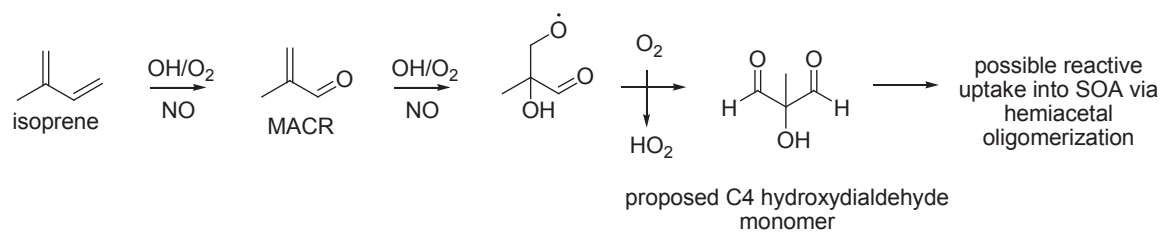


Figure 2.17. Proposed gas-phase formation mechanism for a C₄ hydroxydialdehyde monomer, possibly accounting for a fraction of the unidentified SOA mass in high-NO_x experiments.

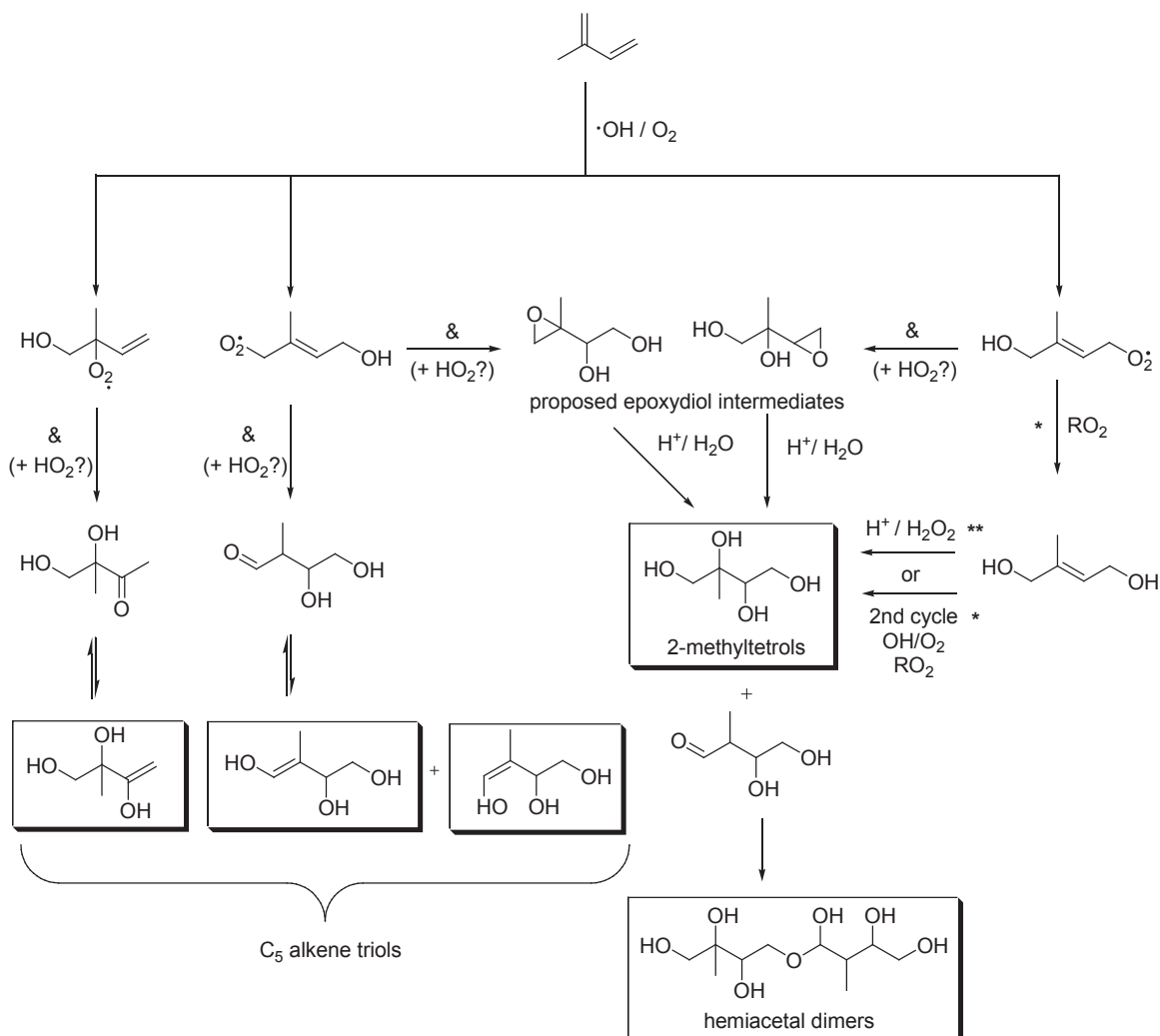


Figure 2.18. Low- NO_x SOA formation pathways as elucidated by GC/MS. Boxes indicate products detected in low- NO_x SOA. Symbols used: $\&$, further study needed for the formations of the hypothetical carbonyl diol and epoxydiol intermediates which may result from the rearrangements of RO_2 radicals and/or hydroperoxides; $*$, for details about this pathway leading to 2-methyltetrols and also holding for isomeric products, see reference 7; $**$, for details about this alternative pathway, see reference 14. 2-methyltetrol performate derivatives (shown in Table 2.4) were omitted for simplicity, however, these could serve as precursors for 2-methyltetrols if in the presence of acid and water.

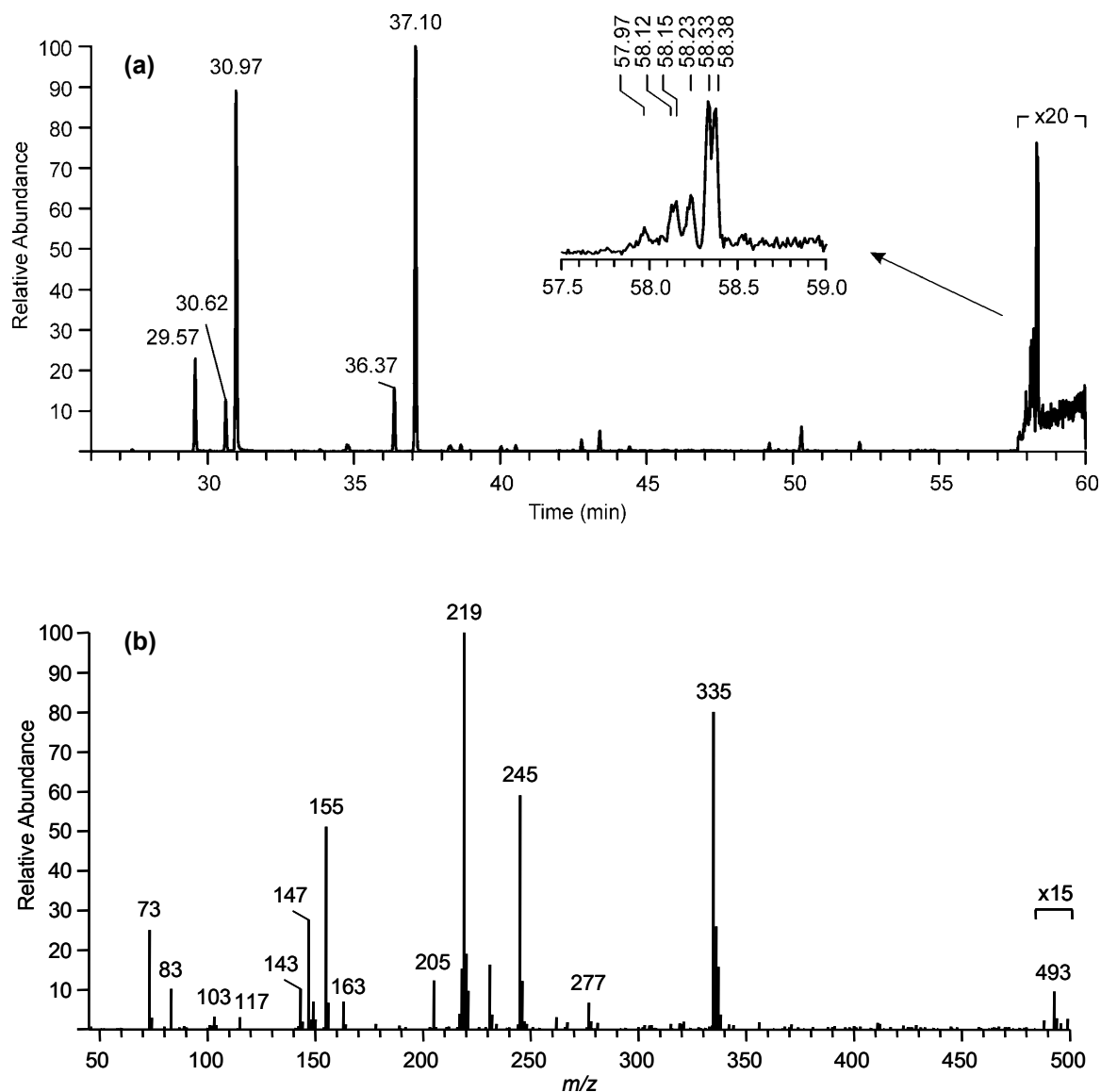
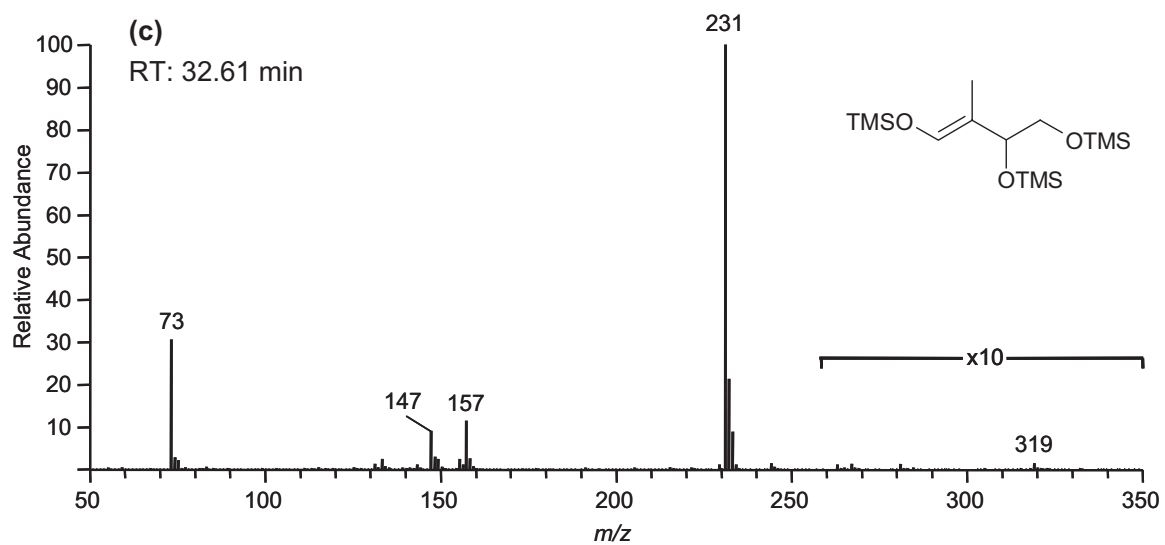
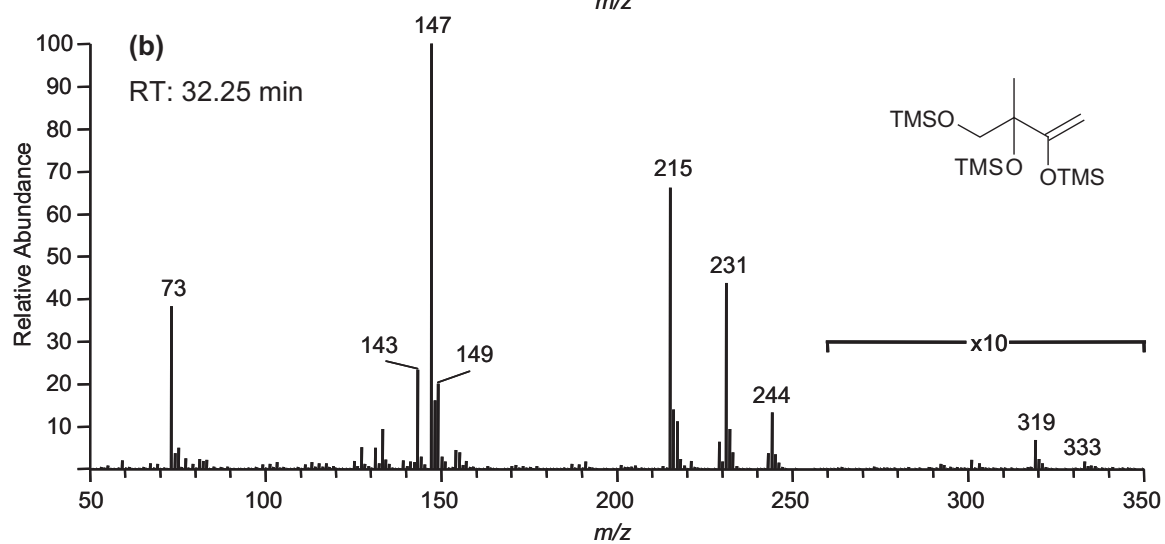
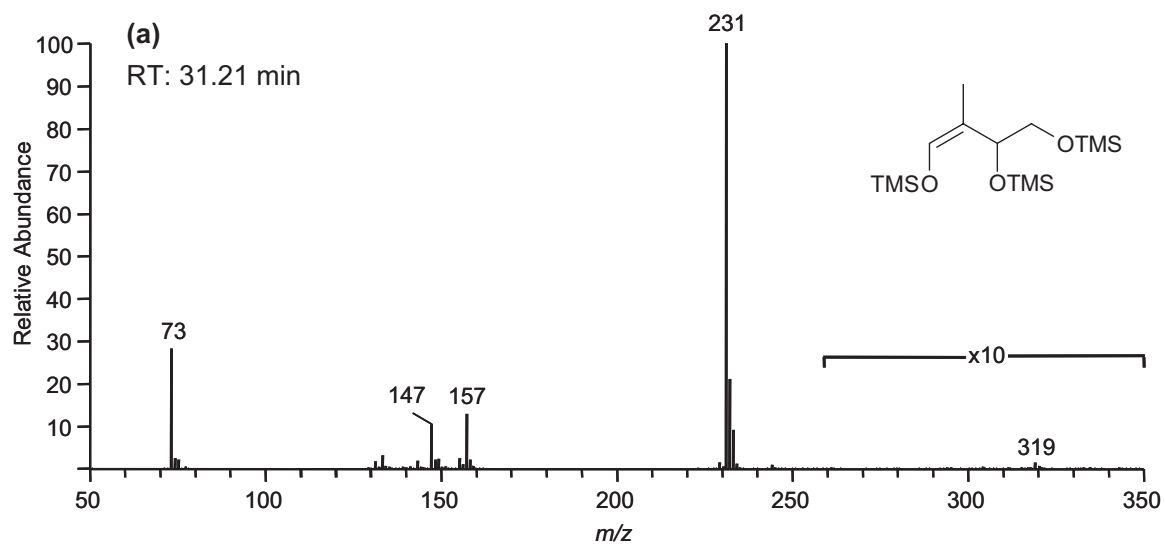
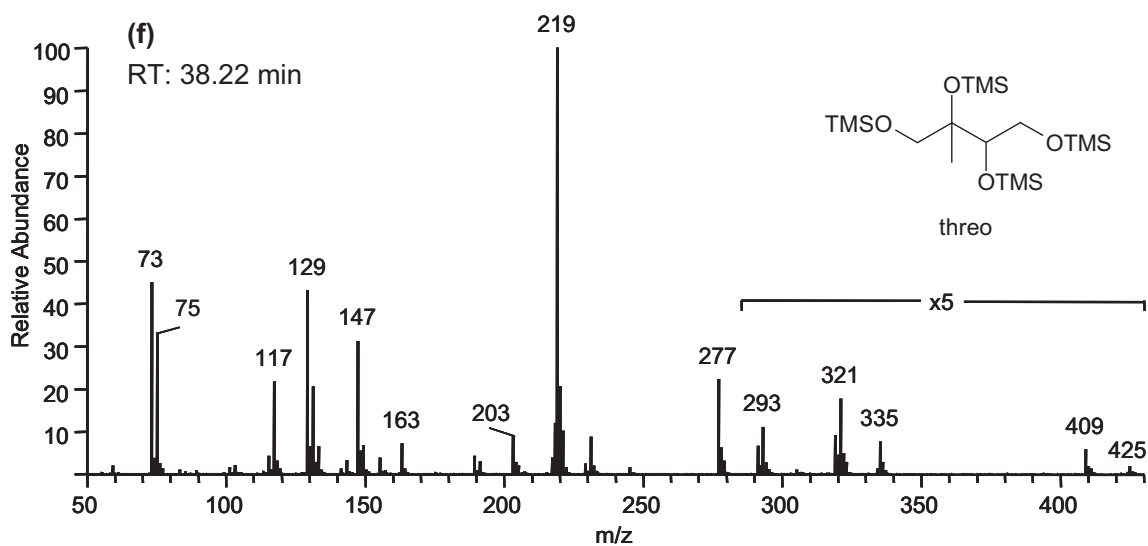
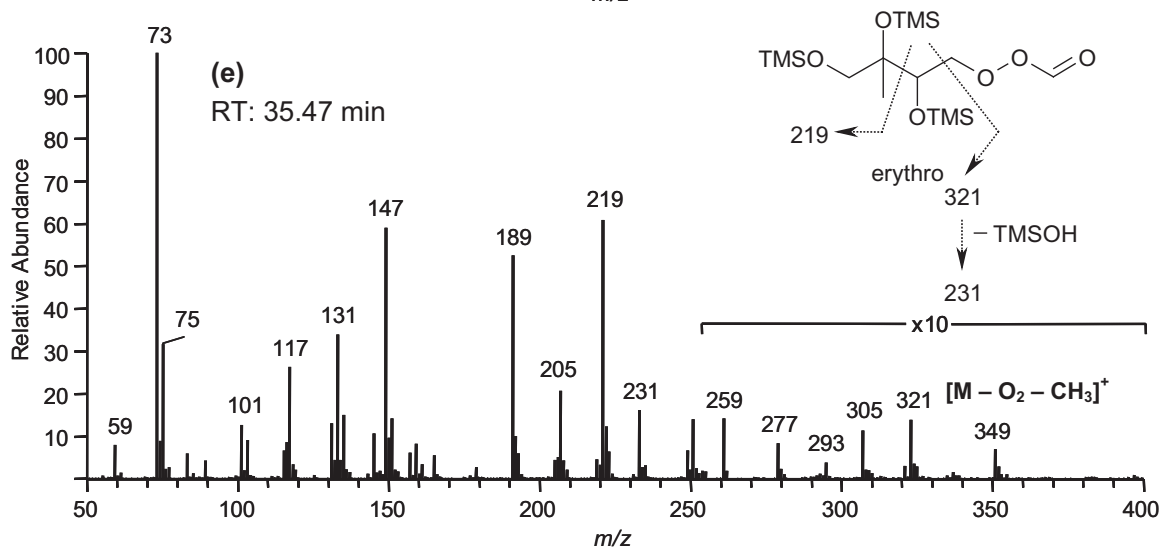
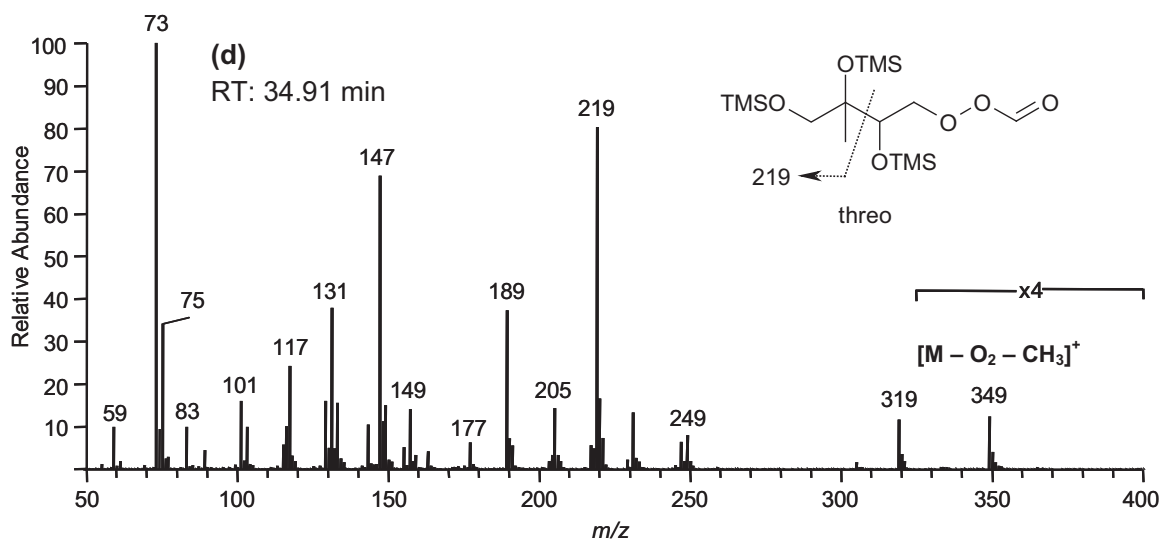


Figure 2.19. (a) GC/MS EIC using specific ions for the TMS derivatives of 2-methyltetrols (m/z 219), C_5 alkene triols (m/z 231), and hemiacetal dimers (m/z 219 and 335) for a $PM_{2.5}$ aerosol sample collected in Rondônia, Brazil, during the onset of the wet season from 10-12 November 2002 (39 h collection time). The insert shows a detail of the isomeric hemiacetal dimers, formed between 2-methyltetrols and C_5 dihydroxycarbonyls, which elute between 57 and 59 min; (b) averaged EI mass spectrum (only limited mass range m/z 50 – 500 available) for the TMS derivatives of the isomeric hemiacetal dimers.





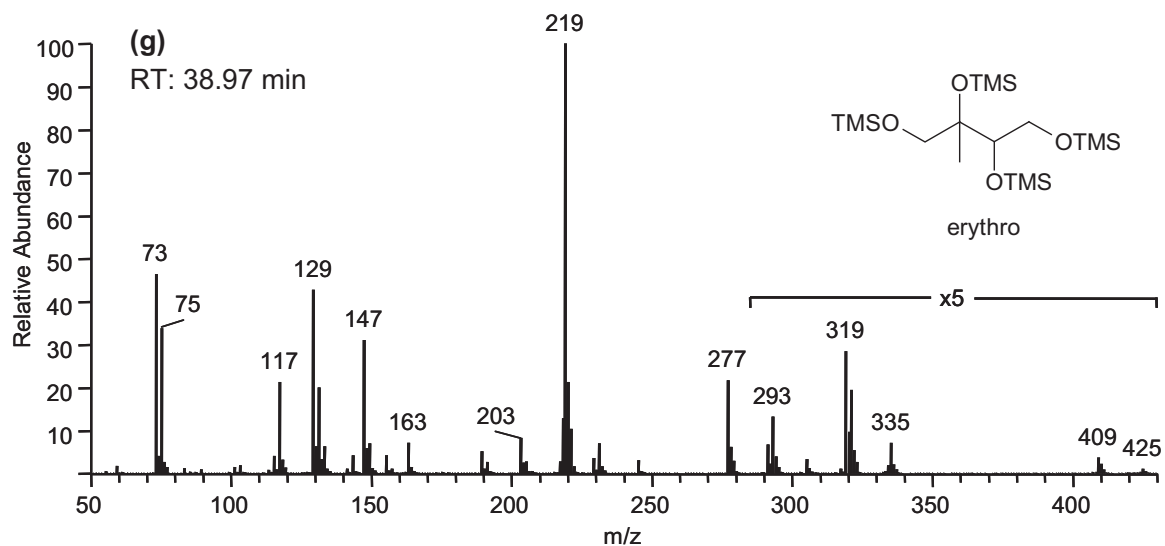


Figure 2.20. EI mass spectra for low-NO_x SOA products detected in the GC/MS TIC of Figure 2.10a. (a), (b), and (c) correspond to mass spectra of isomeric C₅ alkene triols. (d) and (e) correspond to mass spectra of diastereoisomeric 2-methyltetrol performate derivatives. (f) and (g) correspond to mass spectra of diastereoisomeric 2-methyltetrols.